

# Thermal radiation and near-field energy density of thin metallic films

Svend-Age Biehs, Daniel Reddig, and Martin Holthaus

*Institut für Physik and Center of Interface Science,*

*Carl von Ossietzky Universität, D-26111 Oldenburg, Germany*

(Dated: January 31, 2007)

## Abstract

We study the properties of thermal radiation emitted by a thin dielectric slab, employing the framework of macroscopic fluctuational electrodynamics. Particular emphasis is given to the analytical construction of the required dyadic Green's functions. Based on these, general expressions are derived for both the system's Poynting vector, describing the intensity of propagating radiation, and its energy density, containing contributions from non-propagating modes which dominate the near-field regime. An extensive discussion is then given for thin metal films. It is shown that the radiative intensity is maximized for a certain film thickness, due to Fabry–Perot-like multiple reflections inside the film. The dependence of the near-field energy density on the distance from the film's surface is governed by an interplay of several length scales, and characterized by different exponents in different regimes. In particular, this energy density remains finite even for arbitrarily thin films. This unexpected feature is associated with the film's low-frequency surface plasmon polariton. Our results also serve as reference for current near-field experiments which search for deviations from the macroscopic approach.

PACS numbers: 44.40.+a, 78.66.-w, 05.40.-a, 41.20.Jb

## I. INTRODUCTION

A piece of nonmagnetic, linear and isotropic dielectric material with frequency-dependent permittivity  $\varepsilon(\omega)$  kept at some finite temperature  $T$  generates and emits an electromagnetic field, which manifests itself as heat radiation, resulting from thermal and quantum mechanical fluctuations. Besides the thermal far field, near-field phenomena associated with nonpropagating modes have recently attracted increasing attention [1]. Possibly important effects have been revealed, such as the emergence of both temporal and spatial coherence in the near field of planar thermal sources due to surface waves [2–4]. In addition, the influence of these surface waves on radiative heat transfer and dispersion forces at the subwavelength scale has been investigated [1]. In such studies, one usually considers a simple half-space geometry, or two half-spaces separated by a narrow vacuum gap.

The characteristic length scale for absorption of heat radiation by the material is the skin depth

$$d_{\text{skin}} = \frac{1}{k_0 \text{Im}(\sqrt{\varepsilon_r})}, \quad (1)$$

evaluated at the dominant thermal frequency  $\omega_{\text{th}} = 2.821 k_B T / \hbar$ . We use the notation  $k_0 = \omega/c$ , where  $c$  is the velocity of light in vacuum;  $\varepsilon_r(\omega) = \varepsilon(\omega)/\varepsilon_0$  is the relative permittivity, with  $\varepsilon_0$  denoting the permittivity of the vacuum. Thermal radiation generated inside the material can reach its surface only if it originates from its outermost layer with thickness on the order of  $d_{\text{skin}}$ . Hence, if the linear dimensions of a given dielectric are significantly larger than the skin depth, the emitted radiation preserves no information about the material's geometry. In that case, radiating and non-radiating components of the thermal electromagnetic field equal those emitted by a dielectric half-space [5, 6].

In this paper we investigate a seminal example which shows that measurable effects occur when the above two length scales become comparable, so that the half-space model becomes inadequate. We consider an infinite, planar dielectric slab and study the dependence of both its thermal far and near field on its thickness  $d$ . When  $d$  is large compared to  $d_{\text{skin}}$ , the propagating radiation emitted by the slab is described by the Planck–Kirchhoff radiation law [5]. However, when  $d$  is reduced below  $d_{\text{skin}}$ , two competing trends arise: On the one hand, multiple reflections of radiation inside the slab lead to a Fabry–Perot-like enhancement of the field; on the other, the radiating source volume is diminished. We work out the consequences of this competition and show that, in particular, the near-field energy density

close to the surface of a metal film can remain finite even when the thickness of that film becomes arbitrarily small, as a result of the emergence of a low-frequency surface plasmon polariton.

We proceed as follows: In Section II we briefly collect the required elements of fluctuational macroscopic electrodynamics [7], and outline in Sec. III the construction of the classical dyadic Green's functions for the dielectric slab; these turn out to be significantly more complicated than the more often considered ones for a half-space, or for a vacuum gap between two half-spaces [8]. Although properties of propagating thermal radiation may also be obtained by more direct means [9], and numerical codes for investigating thermal radiation of layered structures do exist [10], the detailed analytical discussion of these Green's functions is of its own intrinsic value. Green's functions for layered media appear in a variety of contexts, such as van der Waals forces in multilayer systems [11, 12], magnetic noise in conducting slabs [13], light scattering and control of spontaneous emission in planar cavities [14, 15], or thermal spin flips in atoms chips [16], to name but a few. Unfortunately, the algebra involved in writing down such Green's functions, though not difficult in principle, is vexatingly cumbersome. Here we resort to the formalism outlined in Ref. [17], based on the systematic use of vector wave functions [18], which combines versatility with transparency, and which allows us to treat both far-field and near-field effects on equal footing. With the help of the Green's functions we then derive in Sec. IV general expressions for both the intensity of the slab's thermal radiation field and its energy density, deferring tedious mathematical details to the Appendix A. Section V contains an extensive discussion of these results.

For the sake of definiteness we concentrate on dielectric slabs effectuating a coupling between plasma-like electron motion and the photon field [19], such as metals. Within the Drude approach, their permittivity is given by

$$\varepsilon(\omega) = \varepsilon_0 \left[ 1 + \frac{i}{\omega} \frac{\omega_p^2 \tau}{(1 - i\omega\tau)} \right], \quad (2)$$

where  $\omega_p$  denotes the plasma frequency, and  $\tau$  the relaxation time [20]. Since the dominant thermal frequency amounts to  $\omega_{\text{th}} \approx 1.1 \cdot 10^{14} \text{ s}^{-1}$  for  $T = 300 \text{ K}$ , and since typical relaxation times for metals are on the order of  $10^{-14} \text{ s}$ , one can satisfy the inequality  $\omega\tau \ll 1$  in the infrared, thus arriving at the Hagen–Rubens approximation [21]

$$\varepsilon_r(\omega) = 1 - (\omega_p\tau)^2 + i \frac{\omega_p^2 \tau}{\omega} \quad (3)$$

for the relative permittivity. For metals with comparatively short relaxation time, such as Bismuth ( $\tau_{\text{Bi}} \approx 2.3 \cdot 10^{-16}$  s at  $T = 273$  K), this approximation is quite good indeed. However, a Drude metallic state can also be achieved with conducting polymers; for instance, hexafluorophosphate doped polypyrrole [PPy(PF<sub>6</sub>)] yields a plasma frequency in the far infrared at about  $2 \cdot 10^{13}$  s<sup>-1</sup>, combined with an anomalously long scattering time quantified as  $3 \cdot 10^{-11}$  s in Ref. [22]. Hence, while we use this approximation (3) for deriving various analytical estimates, we rely on the full Drude permittivity (2) in our numerical calculations. Besides Bismuth, for which  $\omega_p \tau \approx 4.8$  at room temperature, we will also consider more typical metals, for which  $\omega_p \tau$  is two orders of magnitude larger.

We consider in subsection VB the radiative intensity emitted by thin metal films, and demonstrate that the opposing trends hinted at above result in an optimum film thickness which maximizes that intensity. We then study in subsection VC the “evanescent” near-field energy density, and establish a somewhat counterintuitive result: While the contribution of the TE modes to that density vanishes when the film thickness goes to zero, that of the TM modes does not, but remains finite and becomes universal, at least within the scope of the simple Drude approach. Finally, we briefly spell out some experimental ramifications in Sec. VI.

## II. ELEMENTS OF FLUCTUATIONAL ELECTRODYNAMICS

As is customary, we consider the macroscopic electric and magnetic fields inside the dielectric material,  $\mathbf{E}(\mathbf{r}, t)$  and  $\mathbf{H}(\mathbf{r}, t)$ , obtained by averaging the microscopic fields over some appropriate volume [23], so that their small-scale, “atomic” fluctuations are smoothed out. Since these fields are described by real numbers, one has

$$\begin{aligned} \mathbf{E}(\mathbf{r}, t) &= \int_{-\infty}^{+\infty} \frac{d\omega}{2\pi} \mathbf{E}(\mathbf{r}, \omega) e^{-i\omega t} \\ &= \int_0^{+\infty} \frac{d\omega}{2\pi} \mathbf{E}(\mathbf{r}, \omega) e^{-i\omega t} + \text{c.c.} , \end{aligned} \quad (4)$$

where c.c. denotes the complex conjugate of the preceding term. A corresponding identity holds for  $\mathbf{H}(\mathbf{r}, t)$ . Hence, it suffices to restrict the temporal Fourier transforms  $\mathbf{E}(\mathbf{r}, \omega)$  and  $\mathbf{H}(\mathbf{r}, \omega)$  to positive frequencies  $\omega$ .

Following Rytov and co-workers [7], we describe the connection between the electromagnetic field and its sources by augmenting the dynamical macroscopic Maxwell equations by

fluctuating current fields. For nonmagnetic materials, characterized by the permeability  $\mu_0$  of the vacuum, only an “electric” current is required, the frequency components  $\mathbf{j}(\mathbf{r}, \omega)$  of which are regarded as independent stochastic variables. The resulting equations

$$\nabla \times \mathbf{E}(\mathbf{r}, \omega) = i\omega\mu_0\mathbf{H}(\mathbf{r}, \omega) \quad (5)$$

$$\nabla \times \mathbf{H}(\mathbf{r}, \omega) = -i\omega\varepsilon(\omega)\mathbf{E}(\mathbf{r}, \omega) + \mathbf{j}(\mathbf{r}, \omega) \quad (6)$$

then adopt the status of Langevin-type stochastic equations, with  $\mathbf{j}(\mathbf{r}, \omega)$  playing the role of a stochastic force. As in the theory of Brownian motion, the correlation functions of these “forces” then are of central importance. As a consequence of the fluctuation-dissipation theorem, they acquire the forms [24, 25]

$$\begin{aligned} \langle j_\alpha(\mathbf{r}, \omega) j_\beta(\mathbf{r}', \omega') \rangle &= 0 \\ \langle j_\alpha(\mathbf{r}, \omega) \overline{j_\beta(\mathbf{r}', \omega')} \rangle &= 4\pi\omega E(\omega, \beta) \varepsilon''(\omega) \delta_{\alpha\beta} \delta(\mathbf{r} - \mathbf{r}') \delta(\omega - \omega') \\ \langle \overline{j_\alpha(\mathbf{r}, \omega)} \overline{j_\beta(\mathbf{r}', \omega')} \rangle &= 0, \end{aligned} \quad (7)$$

where angular brackets indicate an ensemble average, overbars denote complex conjugation, Greek letters specify vector components, and

$$E(\omega, \beta) = \frac{\hbar\omega}{e^{\beta\hbar\omega} - 1} \quad (8)$$

is the mean thermal energy of a quantum mechanical harmonic oscillator with frequency  $\omega$ , omitting the vacuum contribution. As usual,  $\beta = (k_B T)^{-1}$  is the inverse temperature variable;  $\varepsilon''(\omega)$  is the imaginary part of the material’s permittivity  $\varepsilon(\omega) = \varepsilon'(\omega) + i\varepsilon''(\omega)$ .

Since the stochastic Maxwell equations are linear, there exists a linear relationship between the fluctuating sources and the generated fields, which we write as

$$\mathbf{E}(\mathbf{r}, \omega) = i\omega\mu_0 \int d^3r' \mathbf{G}^E(\mathbf{r}, \mathbf{r}', \omega) \cdot \mathbf{j}(\mathbf{r}', \omega), \quad (9)$$

$$\mathbf{H}(\mathbf{r}, \omega) = i\omega\mu_0 \int d^3r' \mathbf{G}^H(\mathbf{r}, \mathbf{r}', \omega) \cdot \mathbf{j}(\mathbf{r}', \omega). \quad (10)$$

The dyadic kernels  $\mathbf{G}^E(\mathbf{r}, \mathbf{r}', \omega)$  and  $\mathbf{G}^H(\mathbf{r}, \mathbf{r}', \omega)$  are referred to as the classical electric and magnetic Green’s function, respectively. Once these kernels are known for the given geometry, the correlation functions (7) allow one to evaluate bilinear expressions of the fields such as

$$\langle E_\alpha(\mathbf{r}, t) H_\beta(\mathbf{r}, t) \rangle = \frac{\mu_0^2}{\pi} \int_0^\infty d\omega \omega^3 E(\omega, \beta) \varepsilon''(\omega) \int d^3r' \left( \mathbf{G}^E \cdot \overline{\mathbf{G}^H} \right)_{\alpha\beta} + \text{c.c.}, \quad (11)$$

which enter into the definition of basic observables, such as the Poynting vector of the thermal radiation emitted by the material, or its energy density. In the following section, we outline the construction of such Green's functions for a dielectric layer of finite thickness. Readers not interested in the mathematical details of this construction can proceed to Sec. IV.

### III. CONSTRUCTION OF DYADIC GREEN'S FUNCTIONS

The electric dyadic Green's function obeys the inhomogeneous vector wave equation [17]

$$\nabla \times \nabla \times \mathbf{G}^E(\mathbf{r}, \mathbf{r}', \omega) - k^2 \mathbf{G}^E(\mathbf{r}, \mathbf{r}', \omega) = \mathbf{1} \delta(\mathbf{r} - \mathbf{r}') , \quad (12)$$

where

$$k^2 = \frac{\omega^2}{c^2} \varepsilon_r(\omega) \quad (13)$$

is the square of the wave number inside a material with relative permittivity  $\varepsilon_r(\omega) = \varepsilon(\omega)/\varepsilon_0$ . Besides, the Green's function also has to satisfy the proper boundary conditions for the respective geometry. For nonmagnetic materials, as considered here, the magnetic Green's function is then easily obtained from the electric one through the relation

$$\mathbf{G}^H = \frac{1}{i\omega\mu_0} \nabla \times \mathbf{G}^E . \quad (14)$$

For constructing Green's functions, one starts from solutions  $\mathbf{V}$  to the homogeneous vector wave equation

$$\nabla \times \nabla \times \mathbf{V} - k^2 \mathbf{V} = \mathbf{0} . \quad (15)$$

Assuming cylindrical symmetry in planes orthogonal to the  $z$ -axis, the appropriate solutions are provided by the vector wave functions [17]

$$\mathbf{M}_{\pm n \lambda}(h) = \left( \mp n \frac{J_n(\lambda \rho)}{\rho} \begin{Bmatrix} \sin \\ \cos \end{Bmatrix} (n\varphi) \mathbf{e}_\rho - \frac{\partial J_n(\lambda \rho)}{\partial \rho} \begin{Bmatrix} \cos \\ \sin \end{Bmatrix} (n\varphi) \mathbf{e}_\varphi \right) e^{ihz} \quad (16)$$

$$\begin{aligned} \mathbf{N}_{\pm n \lambda}(h) = & \left( \frac{ih}{k} \frac{\partial J_n(\lambda \rho)}{\partial \rho} \begin{Bmatrix} \cos \\ \sin \end{Bmatrix} (n\varphi) \mathbf{e}_\rho \mp \frac{ihn}{k} \frac{J_n(\lambda \rho)}{\rho} \begin{Bmatrix} \sin \\ \cos \end{Bmatrix} (n\varphi) \mathbf{e}_\varphi \right. \\ & \left. + \frac{\lambda^2}{k} J_n(\lambda \rho) \begin{Bmatrix} \cos \\ \sin \end{Bmatrix} (n\varphi) \mathbf{e}_z \right) e^{ihz} . \end{aligned} \quad (17)$$

Here,  $J_n(\lambda \rho)$  denotes an ordinary Bessel function of order  $n$ ; the upper (lower) trigonometric function goes with the respective upper (lower) sign. The integer  $n = 0, 1, 2, 3, \dots$  is a

discrete mode index, whereas the real, wave number-like index  $0 \leq \lambda < \infty$  is continuous. This wave-number index refers to propagation orthogonal to the  $z$ -axis, and determines the wave number  $h$  for propagation in  $z$ -direction through the relation

$$\lambda^2 + h^2 = k^2 ; \quad (18)$$

observe that, in contrast to  $\lambda$ , this wave number  $h$  generally is complex. It appears as the argument of the above vector functions, whereas the cylindrical coordinates  $(\rho, \varphi, z)$  of  $\mathbf{r}$  are suppressed. The functions  $\mathbf{M}_{\pm n\lambda}(h)$  are associated with ( $\sigma$ -polarized) TE modes, the functions  $\mathbf{N}_{\pm n\lambda}(h)$  with ( $\pi$ -polarized) TM modes. Besides solving the homogeneous wave equation (15), these functions (16) and (17) also satisfy the useful identities

$$\begin{aligned} \nabla \times \mathbf{M}_{\pm n\lambda}(h) &= k\mathbf{N}_{\pm n\lambda}(h) \\ \nabla \times \mathbf{N}_{\pm n\lambda}(h) &= k\mathbf{M}_{\pm n\lambda}(h) . \end{aligned} \quad (19)$$

It should be pointed out that, besides the vector functions of the  $\mathbf{M}$ - and  $\mathbf{N}$ -type, there also exists a third type denoted  $\mathbf{L}$ . These functions obey  $\nabla \times \mathbf{L} = \mathbf{0}$  and are not needed in the present macroscopic approach [16, 18].

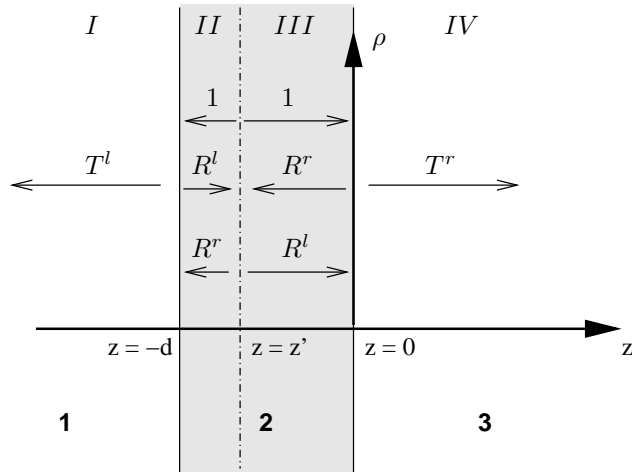


FIG. 1: Slab geometry considered in this work. The region  $-d \leq z \leq 0$  is occupied by a dielectric with permittivity  $\varepsilon_2$ . The permittivities for  $z < -d$  and  $z > 0$  are given by  $\varepsilon_1$  and  $\varepsilon_3$ , respectively. A source at  $z = z'$  within the slab emits radiation with unit amplitude in both directions. One also has to account for waves reflected and transmitted at both interfaces, with amplitudes as indicated, both for TE and TM modes.

We now consider the geometry depicted in Fig. 1: The layer between the infinite planes  $z = 0$  and  $z = -d$  is filled by a dielectric with permittivity  $\varepsilon_2 = \varepsilon_2(\omega)$ ; in this layer we have stochastic source currents generating the electromagnetic field. For later convenience, we do not yet assume at this point that the layer is embedded in a vacuum, but rather that the region  $z < -d$  be occupied by another dielectric with permittivity  $\varepsilon_1$ , while the half-space  $z > 0$  be characterized by still another permittivity  $\varepsilon_3$ . This will allow us to apply the results obtained here to bulk materials covered by thin coatings [26, 27].

If there were no boundary conditions to respect at the interfaces, but the layer  $-d \leq z \leq 0$  were extended to fill the entire three-dimensional space, the dyadic electric Green's function with boundary conditions at  $z = \pm\infty$  specifying “outgoing” waves could directly be adapted from the literature [17]: For  $z > z'$ , one then has

$$\mathbf{G}_0(\mathbf{r}, \mathbf{r}', \omega) = \frac{i}{4\pi} \int_0^\infty d\lambda \sum_{n=0}^\infty \frac{2 - \delta_{n,0}}{\lambda h_2} \left\{ \mathbf{M}_{\pm n\lambda}(h_2) \otimes \mathbf{M}'_{\pm n\lambda}(-h_2) + \mathbf{N}_{\pm n\lambda}(h_2) \otimes \mathbf{N}'_{\pm n\lambda}(-h_2) \right\}, \quad (20)$$

whereas the signs of the arguments  $\pm h_2$  of all four vector functions have to be reversed when  $z < z'$ . Here and in the following, an unprimed vector function  $\mathbf{M}$  or  $\mathbf{N}$  always carries the coordinates of the observation point  $\mathbf{r}$ , whereas a primed function  $\mathbf{M}'$  or  $\mathbf{N}'$  refers to the source point  $\mathbf{r}'$ . The symbol  $\otimes$  indicates a dyadic (exterior) product. Finally,  $\mathbf{M}_{\pm n\lambda}(h_2) \otimes \mathbf{M}'_{\pm n\lambda}(-h_2)$  is a shorthand notation for  $\mathbf{M}_{+n\lambda}(h_2) \otimes \mathbf{M}'_{+n\lambda}(-h_2) + \mathbf{M}_{-n\lambda}(h_2) \otimes \mathbf{M}'_{-n\lambda}(-h_2)$ .

For the slab geometry specified in Fig. 1, this function  $\mathbf{G}_0(\mathbf{r}, \mathbf{r}', \omega)$  has to be modified such that, apart from outgoing boundary conditions at  $z = \pm\infty$ , also the boundary conditions at the two interfaces can be implemented. To this end, we divide the space into four zones: Assuming the source to be located within the slab, so that  $-d < z' < 0$ , we refer to the region  $-\infty < z < -d$  as zone *I*. Then  $-d \leq z < z'$  is zone *II*, while the remaining piece  $z' < z \leq 0$  of the slab becomes zone *III*, and the positive half space  $z > 0$  is dubbed zone *IV*. Since the tangential component of the electric field is continuous at the interfaces, one requires

$$\mathbf{e}_z \times \mathbf{G}_{I/III}^E = \mathbf{e}_z \times \mathbf{G}_{II/IV}^E; \quad (21)$$

continuity of the magnetic field's tangential components leads to the further boundary conditions

$$\mathbf{e}_z \times \nabla \times \mathbf{G}_{I/III}^E = \mathbf{e}_z \times \nabla \times \mathbf{G}_{II/IV}^E. \quad (22)$$

These requirements can be met with the following, piecewise ansatz: In zone *I* one has only



radiation transmitted through the left interface, directed towards  $z = -\infty$ . Specifying still unknown transmission amplitudes  $T_{TE}^l$  and  $T_{TM}^l$  for the TE and TM modes, respectively, we therefore write the electric Green's function  $\mathbb{G}_I^E(\mathbf{r}, \mathbf{r}', \omega)$  with  $\mathbf{r}$  in this zone in the form

$$\mathbb{G}_I^E = \frac{i}{4\pi} \int_0^\infty d\lambda \sum_{n=0}^\infty \frac{2 - \delta_{n,0}}{\lambda h_2} \cdot \left\{ T_{TE}^l \mathbf{M}_{\pm n\lambda}(-h_1) \otimes \mathbf{M}'_{\pm n\lambda}(h_2) + T_{TM}^l \mathbf{N}_{\pm n\lambda}(-h_1) \otimes \mathbf{N}'_{\pm n\lambda}(h_2) \right\}. \quad (23)$$

In zone *II* there is leftward-directed radiation (with unit amplitude) emitted by the source, but also rightward-moving radiation reflected (with amplitudes  $R_{TE}^l$  and  $R_{TM}^l$ ) from the left interface, together with further, leftward-moving radiation reflected (with amplitudes  $R_{TE}^r$  and  $R_{TM}^r$ ) from the right interface:

$$\mathbb{G}_{II}^E = \frac{i}{4\pi} \int_0^\infty d\lambda \sum_{n=0}^\infty \frac{2 - \delta_{n,0}}{\lambda h_2} \cdot \left\{ \left( \mathbf{M}_{\pm n\lambda}(-h_2) + R_{TE}^l \mathbf{M}_{\pm n\lambda}(h_2) \right) \otimes \mathbf{M}'_{\pm n\lambda}(h_2) + R_{TE}^r \mathbf{M}_{\pm n\lambda}(-h_2) \otimes \mathbf{M}'_{\pm n\lambda}(-h_2) \right. \\ \left. + \left( \mathbf{N}_{\pm n\lambda}(-h_2) + R_{TM}^l \mathbf{N}_{\pm n\lambda}(h_2) \right) \otimes \mathbf{N}'_{\pm n\lambda}(h_2) + R_{TM}^r \mathbf{N}_{\pm n\lambda}(-h_2) \otimes \mathbf{N}'_{\pm n\lambda}(-h_2) \right\}. \quad (24)$$

In zone *III* one has, *mutatis mutandis*, the same dynamics as in zone *II*, giving

$$\mathbb{G}_{III}^E = \frac{i}{4\pi} \int_0^\infty d\lambda \sum_{n=0}^\infty \frac{2 - \delta_{n,0}}{\lambda h_2} \cdot \left\{ \left( \mathbf{M}_{\pm n\lambda}(h_2) + R_{TE}^r \mathbf{M}_{\pm n\lambda}(-h_2) \right) \otimes \mathbf{M}'_{\pm n\lambda}(-h_2) + R_{TE}^l \mathbf{M}_{\pm n\lambda}(h_2) \otimes \mathbf{M}'_{\pm n\lambda}(h_2) \right. \\ \left. + \left( \mathbf{N}_{\pm n\lambda}(h_2) + R_{TM}^r \mathbf{N}_{\pm n\lambda}(-h_2) \right) \otimes \mathbf{N}'_{\pm n\lambda}(-h_2) + R_{TM}^l \mathbf{N}_{\pm n\lambda}(h_2) \otimes \mathbf{N}'_{\pm n\lambda}(h_2) \right\}, \quad (25)$$

whereas zone *IV* provides a mirror image of zone *I*:

$$\mathbb{G}_{IV}^E = \frac{i}{4\pi} \int_0^\infty d\lambda \sum_{n=0}^\infty \frac{2 - \delta_{n,0}}{\lambda h_2} \cdot \left\{ T_{TE}^r \mathbf{M}_{\pm n\lambda}(h_3) \otimes \mathbf{M}'_{\pm n\lambda}(-h_2) + T_{TM}^r \mathbf{N}_{\pm n\lambda}(h_3) \otimes \mathbf{N}'_{\pm n\lambda}(-h_2) \right\}. \quad (26)$$

Of course, the above ansatz is characterized in mathematical terms by stating that a suitable solution of the homogeneous vector wave equation (15) has been added to the particular solution (20) of the inhomogeneous equation (12).

We are now left with eight unknowns  $T_{TE, TM}^{r,l}$  and  $R_{TM, TE}^{r,l}$ , which match the number of boundary conditions provided by Eqs. (21) and (22), since these apply independently to both

the TE and the TM modes. We concentrate on the radiation field in zone *IV*, and therefore evaluate the transmission coefficients  $T_{TE}^r$  and  $T_{TM}^r$ . This procedure is quite cumbersome, but elementary, so we immediately proceed to the result: The contribution of the TE modes to the radiation emitted by the slab into zone *IV* is determined by

$$T_{TE}^r \mathbf{M}(h_3) \otimes \mathbf{M}'(-h_2) = \frac{2h_2}{D_\perp} \left[ (h_1 + h_2) e^{-ih_2 d} \mathbf{M}(h_3) \otimes \mathbf{M}'(-h_2) - (h_1 - h_2) e^{ih_2 d} \mathbf{M}(h_3) \otimes \mathbf{M}'(h_2) \right], \quad (27)$$

while that of the TM modes follows from

$$T_{TM}^r \mathbf{N}(h_3) \otimes \mathbf{N}'(-h_2) = \frac{2h_2 k_2}{D_\parallel k_3} \left[ \left( h_1 \frac{\varepsilon_2}{\varepsilon_1} + h_2 \right) e^{-ih_2 d} \mathbf{N}(h_3) \otimes \mathbf{N}'(-h_2) - \left( h_1 \frac{\varepsilon_2}{\varepsilon_1} - h_2 \right) e^{ih_2 d} \mathbf{N}(h_3) \otimes \mathbf{N}'(h_2) \right]. \quad (28)$$

For ease of notation, we henceforth omit the mode indices “ $\pm n\lambda$ ” from the vector wave functions, and use the determinants

$$D_\perp = (h_1 + h_2)(h_3 + h_2) e^{-ih_2 d} - (h_1 - h_2)(h_3 - h_2) e^{ih_2 d} \quad (29)$$

and

$$D_\parallel = \left( h_1 \frac{\varepsilon_2}{\varepsilon_1} + h_2 \right) \left( h_3 \frac{\varepsilon_2}{\varepsilon_3} + h_2 \right) e^{-ih_2 d} - \left( h_1 \frac{\varepsilon_2}{\varepsilon_1} - h_2 \right) \left( h_3 \frac{\varepsilon_2}{\varepsilon_3} - h_2 \right) e^{ih_2 d}. \quad (30)$$

Inserting these results (27) and (28) into the electric Green’s function (26), the radiation field existing in the half-space  $z > 0$  is completely specified, since the magnetic Green’s function for that zone is immediately obtained from Eq. (14), keeping in mind the relations (19).

#### IV. THERMAL RADIATION EMITTED BY A DIELECTRIC LAYER

As an application of the above formalism we evaluate the intensity of thermal radiation emitted by the slab into the half-space  $z > 0$ , as given by the  $z$ -component of the Poynting vector,

$$\begin{aligned} \langle S_z(\rho, \varphi, z) \rangle &= \epsilon_{z\beta\gamma} \langle E_\beta(\mathbf{r}, t) H_\gamma(\mathbf{r}, t) \rangle \\ &= \epsilon_{z\beta\gamma} \frac{\mu_0^2}{\pi} \int_0^\infty d\omega \omega^3 E(\omega, \beta) \varepsilon''(\omega) \int d^3 r' \left( \mathbf{G}_{IV}^E \cdot \overline{\mathbf{G}_{IV}^{H^t}} \right)_{\beta\gamma} + \text{c.c.}, \quad (31) \end{aligned}$$

where  $\epsilon_{z\beta\gamma}$  denotes the Levi-Civita tensor. The calculation is not trivial and involves several algebraic manipulations also encountered when computing the field’s energy density, so we

collect the main steps in Appendix A. Because of translational symmetry in planes parallel to the interfaces, the result does not depend on the cylindrical coordinates  $\rho, \varphi$  :

$$\langle S_z(z) \rangle = \int_0^\infty d\omega \frac{E(\omega, \beta)}{(2\pi)^2} \int_0^\infty d\lambda \lambda e^{-2h_3''z} (T_\perp + T_\parallel) , \quad (32)$$

where  $h_3''$  is the imaginary part of the wave number  $h_3 = h_3' + ih_3''$ , and the dimensionless transmission coefficients  $T_\perp$  and  $T_\parallel$  are given by

$$T_\perp = \frac{4\text{Re}(h_3)}{|D_\perp|^2} \left[ \text{Re}(h_2)A_\perp + \text{Im}(h_2)B_\perp \right] \quad (33)$$

$$T_\parallel = \frac{4\text{Re}(h_3\bar{\varepsilon}_{r3})}{|D_\parallel|^2|\varepsilon_{r3}|^2} \left[ \text{Re}(h_2\bar{\varepsilon}_{r2})A_\parallel + \text{Im}(h_2\bar{\varepsilon}_{r2})B_\parallel \right] , \quad (34)$$

employing the relative permittivities  $\varepsilon_{rj} = \varepsilon_j(\omega)/\varepsilon_0$ , together with the auxiliary, real quantities

$$\begin{aligned} A_\perp &= |h_1 + h_2|^2 (e^{2h_2''d} - 1) + |h_1 - h_2|^2 (1 - e^{-2h_2''d}) \\ A_\parallel &= \left| h_1 \frac{\varepsilon_2}{\varepsilon_1} + h_2 \right|^2 (e^{2h_2''d} - 1) + \left| h_1 \frac{\varepsilon_2}{\varepsilon_1} - h_2 \right|^2 (1 - e^{-2h_2''d}) \end{aligned} \quad (35)$$

and

$$\begin{aligned} B_\perp &= 2\text{Im} \left( (h_1 + h_2) \overline{(h_1 - h_2)} (e^{-2ih_2'd} - 1) \right) \\ B_\parallel &= 2\text{Im} \left( \left( h_1 \frac{\varepsilon_2}{\varepsilon_1} + h_2 \right) \overline{\left( h_1 \frac{\varepsilon_2}{\varepsilon_1} - h_2 \right)} (e^{-2ih_2'd} - 1) \right) . \end{aligned} \quad (36)$$

In the case of thick layers, where  $h_2''d \rightarrow \infty$ , one has

$$\begin{aligned} \frac{A_\perp}{|D_\perp|^2} &\rightarrow \frac{1}{|h_3 + h_2|^2} , & \frac{B_\perp}{|D_\perp|^2} &\rightarrow 0 , \\ \frac{A_\parallel}{|D_\parallel|^2} &\rightarrow \frac{1}{\left| h_3 \frac{\varepsilon_2}{\varepsilon_3} + h_2 \right|^2} , & \frac{B_\parallel}{|D_\parallel|^2} &\rightarrow 0 , \end{aligned} \quad (37)$$

so that one recovers the well-known coefficients which determine the radiation emitted by a bulk material with planar surface [2, 5–7]:

$$\begin{aligned} T_\perp &\rightarrow \frac{4\text{Re}(h_3)\text{Re}(h_2)}{|h_3 + h_2|^2} \\ T_\parallel &\rightarrow \frac{4\text{Re}(h_3\bar{\varepsilon}_{r3})\text{Re}(h_2\bar{\varepsilon}_{r2})}{\left| h_3 \frac{\varepsilon_2}{\varepsilon_3} + h_2 \right|^2 |\varepsilon_{r3}|^2} . \end{aligned} \quad (38)$$

The opposite limiting case of very thin layers, with  $h'_2 d \rightarrow 0$  and  $h''_2 d \rightarrow 0$ , is less obvious. After some tedious algebra, one finds

$$\begin{aligned} T_{\perp} &\rightarrow \frac{4\text{Re}(h_3)d\varepsilon''_{r2}k_0^2}{|h_1+h_3|^2} \\ T_{\parallel} &\rightarrow \frac{4\text{Re}(h_3\bar{\varepsilon}_{r3})d\varepsilon''_{r2}}{\left|h_1\frac{\varepsilon_2}{\varepsilon_1}+h_3\frac{\varepsilon_2}{\varepsilon_3}\right|^2|\varepsilon_{r3}|^2}\left(\left|h_1\frac{\varepsilon_2}{\varepsilon_1}\right|^2+\lambda^2\right), \end{aligned} \quad (39)$$

with  $k_0 = \omega/c$ . If both  $\varepsilon_1(\omega) = \varepsilon_0$  and  $\varepsilon_3(\omega) = \varepsilon_0$ , so that the layer is surrounded by vacuum, this gives

$$\begin{aligned} T_{\perp} &\rightarrow \frac{h'_0 d \varepsilon''_{r2} k_0^2}{|h_0|^2} \\ T_{\parallel} &\rightarrow \frac{h'_0 d \varepsilon''_{r2}}{|h_0|^2 |\varepsilon_{r2}|^2} \left( |h_0|^2 |\varepsilon_{r2}|^2 + \lambda^2 \right). \end{aligned} \quad (40)$$

Since according to Eq. (18) one has  $h'_0 = 0$  for evanescent modes with  $\lambda \geq k_0$ , only propagating modes with  $\lambda < k_0$  contribute to the Poynting vector. It is then a simple matter to invoke Eq. (32) for computing the intensity of thermal radiation emitted by a very thin dielectric layer into the vacuum:

$$\langle S_z \rangle \rightarrow \frac{4}{3} \int_0^{\infty} d\omega \frac{E(\omega, \beta)}{(2\pi)^2} \varepsilon''_{r2} k_0^3 d \left( 1 + \frac{1}{2|\varepsilon_{r2}|^2} \right). \quad (41)$$

As may have been expected, this intensity is proportional to the thickness  $d$  of the source layer; when that thickness goes to zero, there are no sources left and the intensity vanishes. It is also noteworthy that the emitted intensity acquires substantial contributions from frequency intervals within which the layer's permittivity is close to zero [19].

Besides the intensity, a further quantity of interest is the energy density  $\langle u \rangle$  of the electromagnetic field. In contrast to the radiative intensity, this quantity is sensitive also to evanescent modes. Focussing on dielectrics facing the vacuum, so that  $\varepsilon_3(\omega) = \varepsilon_0$ , we then have to evaluate

$$\langle u(z) \rangle = \frac{\varepsilon_0}{2} \langle \mathbf{E}^2 \rangle + \frac{\mu_0}{2} \langle \mathbf{H}^2 \rangle. \quad (42)$$

A calculation which largely parallels the one outlined in Appendix A eventually leads to

$$\langle u(z) \rangle = \frac{1}{2(2\pi c)^2} \int_0^{\infty} d\omega \omega E(\omega, \beta) \int_0^{\infty} d\lambda \lambda e^{-2h'_3 z} \left( 1 + \frac{\lambda^2 + |h_3|^2}{k_0^2} \right) \frac{(T_{\perp} + T_{\parallel})}{h'_3}, \quad (43)$$

where  $\varepsilon_{r3} = 1$  is understood when computing the transmission coefficients (33) and (34).

## V. THERMAL RADIATION EMITTED BY A THIN METALLIC FILM

### A. Transmission coefficients for propagating and evanescent modes

In order to clarify the physical significance of the preceding formal results (32) and (43), we now express the key quantities specifying the radiative properties of the dielectric layer, the transmission coefficients (33) and (34), in terms of the Fresnel amplitude reflection coefficients. For radiation coming from a medium with permittivity  $\varepsilon_1$  and going into one with permittivity  $\varepsilon_2$ , these Fresnel coefficients are given by [23]

$$r_{\perp}^{12} = \frac{h_1 - h_2}{h_1 + h_2} \quad (44)$$

for TE modes, and

$$r_{\parallel}^{12} = \frac{h_1 \frac{\varepsilon_2}{\varepsilon_1} - h_2}{h_1 \frac{\varepsilon_2}{\varepsilon_1} + h_2} \quad (45)$$

for TM modes. Introduction of these quantities necessitates to distinguish explicitly between propagating and evanescent modes. In all of this Section we assume  $\varepsilon_3(\omega) = \varepsilon_0$ , and thus study thermal radiation emitted into the vacuum. Then propagating modes are characterized by  $\lambda < k_0 = \omega/c$ , evanescent ones by  $\lambda \geq k_0$ . Defining four functions

$$\begin{aligned} f &= (1 - e^{-2h_2''d}) + |r^{12}|^2 (e^{-2h_2''d} - e^{-4h_2''d}) \\ g &= 2e^{-2h_2''d} \text{Im} \left( \overline{r^{12}} (e^{-2ih_2'd} - 1) \right), \end{aligned} \quad (46)$$

where both the Fresnel coefficients  $r^{12}$  of the left interface and, hence, also the functions  $f$  and  $g$  themselves carry either the label “ $\perp$ ” or “ $\parallel$ ”, then rearranging the r.h.s. of Eqs. (33) and (34) with  $\varepsilon_{r3} = 1$ , we find their equivalent form

$$T^{\text{pr}} = \frac{1}{|1 - r^{12}r^{32} e^{2ih_2d}|^2} \left[ (1 - |r^{32}|^2)f - 2 \text{Im}(r^{32})g \right] \quad (47)$$

for propagating modes, whereas the corresponding expression for evanescent modes with  $\gamma = \sqrt{\lambda^2 - k_0^2}$  is given by

$$T^{\text{ev}} = \frac{h_3'/\gamma}{|1 - r^{12}r^{32} e^{2ih_2d}|^2} \left[ 2 \text{Im}(r^{32})f + (1 - |r^{32}|^2)g \right], \quad (48)$$

again for both types of polarization. In the case of thick layers,  $h_2''d \gg 1$ , these coefficients reduce to

$$\begin{aligned} T^{\text{pr}} &\rightarrow 1 - |r^{32}|^2 \\ T^{\text{ev}} &\rightarrow \frac{2}{\gamma} \text{Re}(h_3) \text{Im}(r^{32}), \end{aligned} \quad (49)$$

so that one correctly reobtains the familiar expressions describing thermal radiation emitted by a bulk dielectric [2, 5–7].

However, here we are interested in the radiative properties of dielectric films thinner than the skin depth of the material under consideration, so that there are two competing length scales. This case requires substantially more care: Provided  $|h'_2 d| \ll 1$  and  $h''_2 d \ll 1$ , the above functions  $f$  and  $g$  reduce to

$$\begin{aligned} f &\rightarrow 2h''_2 d (1 + |r^{12}|^2) \\ g &\rightarrow -4h'_2 d \operatorname{Re}(r^{12}) \end{aligned} \quad (50)$$

in linear approximation. For strongly evanescent modes with  $\lambda \gg k_0$  one has  $h_2 \approx i\lambda$ , and hence  $h''_2 \gg |h'_2|$ . In the case of propagating modes, a similar hierarchy can be established only if one specifies the film's permittivity  $\varepsilon_2(\omega)$ . In the following discussion, we restrict ourselves to simple metals described by the Drude approach, resulting in the permittivity (2), or in its approximation (3), provided the Hagen–Rubens condition  $\omega\tau \ll 1$  can be met for all relevant frequencies.

Given such a Drude metal, the equality  $\lambda^2 + h_2^2 = k_0^2 \varepsilon_{r2}$  requires  $|h'_2| \ll h''_2$  for thermal frequencies. By means of the approximation (50), one then finds  $|g| \ll f$  for sufficiently thin films, so that contributions proportional to  $g$  may be neglected. Hence, we have

$$\begin{aligned} T^{\text{pr}} &= \frac{2h''_2 d}{|1 - r^{12} r^{32} (1 - 2h''_2 d)|^2} (1 + |r^{12}|^2) (1 - |r^{32}|^2) \\ T^{\text{ev}} &= \frac{2h''_2 d}{|1 - r^{12} r^{32} (1 - 2h''_2 d)|^2} \frac{2h'_3}{\gamma} (1 + |r^{12}|^2) \operatorname{Im}(r^{32}) \end{aligned} \quad (51)$$

for thin metallic films. In terms of the dimensionless variable  $\xi = 2h''_2 d$ , the dependence of both propagating and evanescent thermal radiation on the film thickness is therefore determined by the function

$$\begin{aligned} F(\xi) &= \frac{\xi}{|1 - a(1 - \xi)|^2} \\ &= \frac{\xi}{[1 - a'(1 - \xi)]^2 + a''^2(1 - \xi)^2}, \end{aligned} \quad (52)$$

with  $a = r^{12} r^{32}$ .

## B. Dependence of radiative intensity on film thickness

From here onwards we focus on metallic films in vacuum, so that  $r^{12} = r^{32} \equiv r$ , and first estimate that film thickness  $d_W$  which results in maximum far-field heat radiation due to propagating modes. We consider only modes directed perpendicular to the interfaces, so that  $\lambda = 0$ , and

$$r^2 = \left( \frac{1 - \sqrt{\varepsilon_r}}{1 + \sqrt{\varepsilon_r}} \right)^2 \quad (53)$$

for both types of polarization. The Hagen–Rubens condition  $\omega\tau \ll 1$  entails  $\varepsilon_r'' \gg |\varepsilon_r'|$ , or  $|\varepsilon_r| \approx \varepsilon_r'' \gg 1$ , implying both  $|r'| \approx 1$  and  $|r''| \ll 1$ . With  $a = (r' + ir'')^2$  one deduces  $a' \approx r^2 \approx 1$  and  $|a''| \ll 1$ , so that it suffices to maximize, instead of the function  $F(\xi)$ , its approximate version

$$F^{\text{pr}}(\xi) = \frac{\xi}{\xi^2 + a''^2(1 - \xi)^2}. \quad (54)$$

Since  $|a''| \ll 1$ , the maximum is located at

$$\xi_{\text{max}} \approx |a''|, \quad (55)$$

giving

$$\begin{aligned} d_W &\approx \frac{4 \operatorname{Im} \sqrt{\varepsilon_r}}{2h_2'' \varepsilon_r''} \\ &\approx \frac{2c}{\omega_p^2 \tau} \end{aligned} \quad (56)$$

for the optimum film thickness. This characteristic length (56) coincides exactly with the so-called Woltersdorff thickness, which quantifies that thickness of a metallic film which maximizes its absorption for frequencies  $\omega$  in the Hagen–Rubens regime [21, 28, 29]. Indeed, it has been demonstrated experimentally that metal films absorb more infrared radiation if they are made thinner; for most metals, maximum absorptance is obtained for films less than  $10^{-8}$  m thick [30]. In terms of the skin depth (1), which takes the form

$$d_{\text{skin}} = \frac{c}{\omega_p} \sqrt{\frac{2}{\omega\tau}} \quad (57)$$

for metals in the infrared [21], and using  $k_0 = \omega/c$ , the Woltersdorff thickness can be expressed as

$$d_W = d_{\text{skin}}^2 k_0. \quad (58)$$

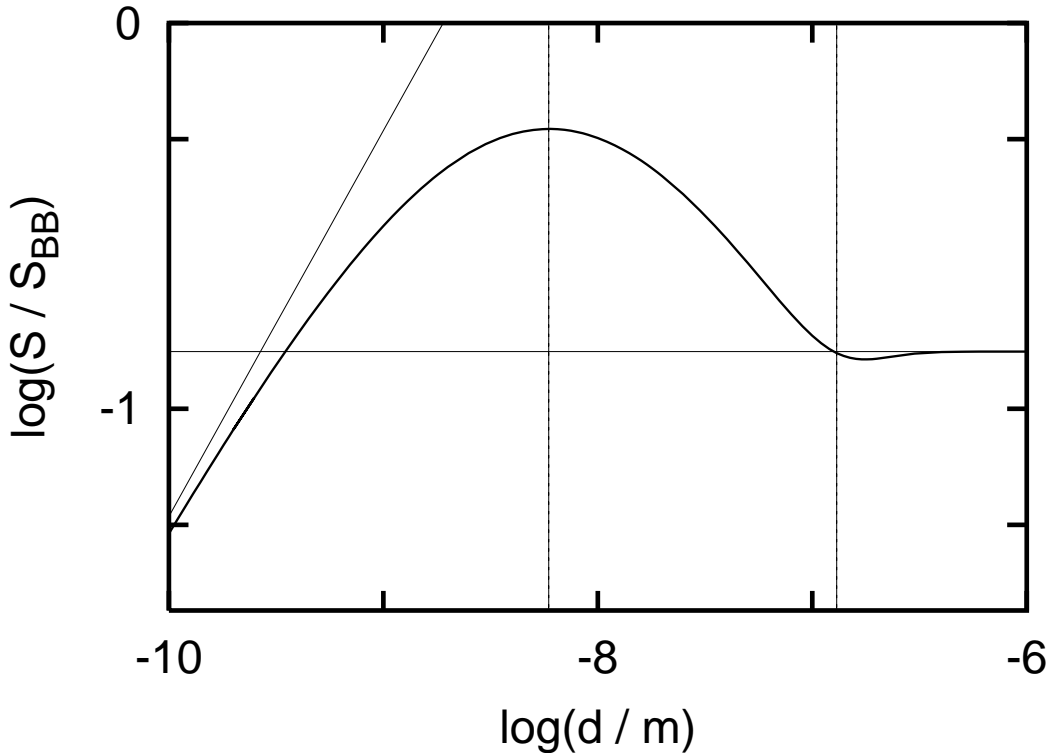


FIG. 2: Radiative intensity  $S$  emitted at temperature  $T = 300$  K by a Drude metal with plasma frequency  $\omega_p = 2.1 \cdot 10^{16} \text{ s}^{-1}$  and relaxation time  $\tau = 2.3 \cdot 10^{-16} \text{ s}$ , as appropriate for Bismuth, as function of the film thickness  $d$  (in meters). Vertical lines indicate the Woltersdorff thickness (56) and the skin depth (1), respectively. Data are normalized with respect to the intensity  $S_{\text{BB}}$  emitted by a black body. Also indicated is the bulk value (horizontal line) and the prediction based on Eq. (41).

The observation that a film of thickness  $d_W$  also maximizes its emission reflects the fact that absorption balances emission in thermal equilibrium.

In Fig. 2 we display numerical data for the radiative intensity emitted at temperature  $T = 300$  K by a Drude metal with parameters  $\omega_p = 2.1 \cdot 10^{16} \text{ s}^{-1}$  and  $\tau = 2.3 \cdot 10^{-16} \text{ s}$  corresponding to Bismuth, as function of the film thickness  $d$ ; in all our numerical calculations we employ the model permittivity (2) without the Hagen–Rubens approximation. Although macroscopic electrodynamics will presumably start to fail for thicknesses below  $10^{-8} \text{ m}$ , we also plot data for even smaller  $d$ , in order to clearly bring out the asymptotic trend. This example confirms the picture drawn so far: The intensity emitted by the film almost coincides with that emitted by the bulk material when  $d$  exceeds the skin depth, but increases



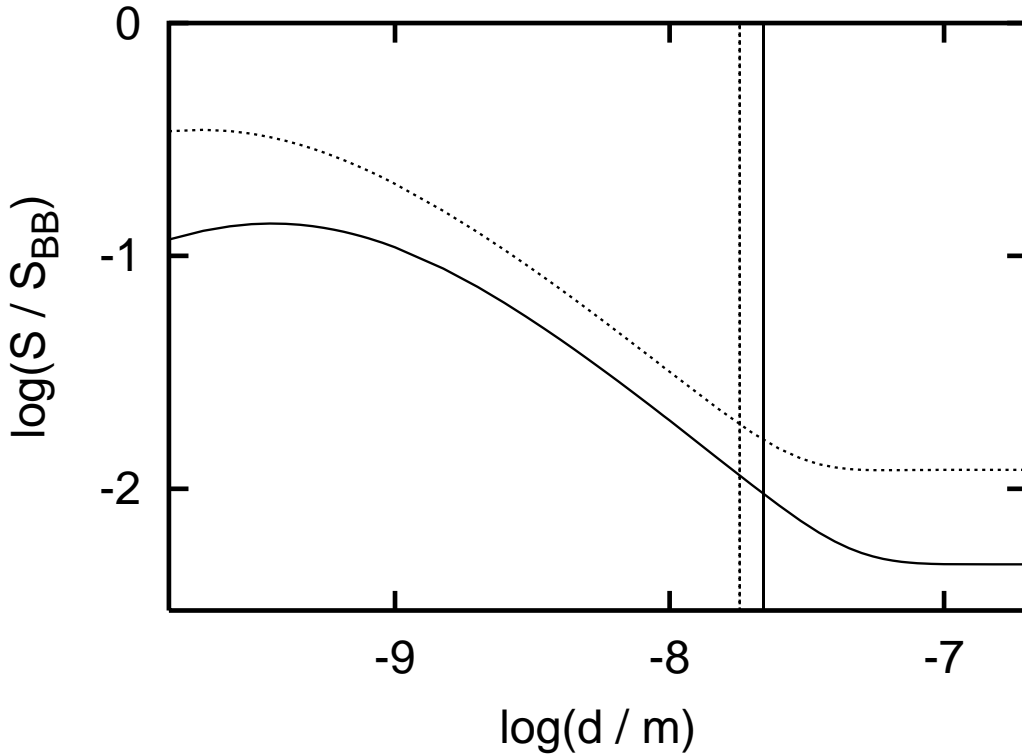


FIG. 3: Radiative intensity  $S$  emitted at temperature  $T = 300$  K by a Drude metal with  $\omega_p = 1.4 \cdot 10^{16} \text{ s}^{-1}$  and  $\tau = 4.0 \cdot 10^{-14} \text{ s}$ , as corresponding to silver (full line), and another such metal with  $\omega_p = 2.4 \cdot 10^{16} \text{ s}^{-1}$  and  $\tau = 0.8 \cdot 10^{-14} \text{ s}$ , as corresponding to aluminium (dotted). Vertical lines mark the corresponding skin depths.

substantially when  $d$  is made smaller, reaching a maximum which exceeds the bulk value by a factor of about 3.8 at a thickness predicted neatly by the Woltersdorff formula (56), and then starting to decrease. However, the regime of linear decrease described by Eq. (41) is reached only for unrealistically small  $d$ . For metals with more typical Drude parameters at room temperature, such as silver ( $\omega_p = 1.4 \cdot 10^{16} \text{ s}^{-1}$  and  $\tau = 4.0 \cdot 10^{-14} \text{ s}$ ) or aluminium ( $\omega_p = 2.4 \cdot 10^{16} \text{ s}^{-1}$  and  $\tau = 0.8 \cdot 10^{-14} \text{ s}$ ), the maximum is shifted to even lower  $d$ , as witnessed by Fig. 3, so that only radiative intensity increasing with decreasing film thickness might be observable in such cases. It is noteworthy that the intensity generated by a thin film can exceed the bulk limit by more than a factor of 10.

### C. Near-field energy density for thin metal films

While the dependence of the radiative intensity on the film thickness thus conforms to expectation, the dependence of the “evanescent” energy density, at some distance  $z$  from the film surface, on that thickness is more difficult to oversee. This is related to the fact that for strongly evanescent modes with  $\lambda \gg k_0$  both Fresnel coefficients (44) and (45) differ strongly: One finds

$$r_{\parallel} \approx \frac{\varepsilon_r - 1}{\varepsilon_r + 1} \quad (59)$$

for  $\lambda/k_0 \gg 1$ , so that

$$\begin{aligned} \operatorname{Re}(r_{\parallel}^2) &\approx 1 - \frac{4\omega^2}{(\omega_p^2\tau)^2} \\ \operatorname{Im}(r_{\parallel}^2) &\approx \frac{4\omega}{\omega_p^2\tau}, \end{aligned} \quad (60)$$

but

$$r_{\perp} \approx \frac{k_0^2 \varepsilon_r - 1}{\lambda^2 \frac{4}{\varepsilon_r}}, \quad (61)$$

giving

$$\begin{aligned} \operatorname{Re}(r_{\perp}^2) &\approx -\frac{k_0^4}{16\lambda^4} \left(\frac{\omega_p^2\tau}{\omega}\right)^2 \\ \operatorname{Im}(r_{\perp}^2) &\approx 2\omega\tau \operatorname{Re}(r_{\perp}^2) \end{aligned} \quad (62)$$

for  $\lambda/k_0 \gg 1$  in the Hagen–Rubens regime. Hence, for strongly evanescent TM modes we have  $\operatorname{Re}(r_{\parallel}^2) \approx 1$  and  $\operatorname{Im}(r_{\parallel}^2) \ll 1$ , which are precisely the propositions which have enabled us to reduce the transmission function (52) to the simpler form (54) for propagating modes. Hence, we can immediately adapt the result obtained in Eq. (55): For evanescent TM modes with  $\lambda/k_0 \gg 1$ , the optimum film thickness maximizing the energy density close to the film’s surface is given by

$$d_{\parallel}^{\text{ev}} \approx \frac{|\operatorname{Im}(r_{\parallel}^2)|}{2h_2''}, \quad (63)$$

which implies

$$k_0 d_{\parallel}^{\text{ev}} \approx \frac{2\omega}{\omega_p^2\tau} \frac{k_0}{\lambda} \quad (64)$$

within the Hagen–Rubens approximation (60), using  $h_2'' \approx \lambda$ . In Fig. 4 we show a plot of the transmission function (52) for evanescent TM modes, obtained for Bismuth parameters with  $\omega$  kept fixed at the dominant thermal frequency  $\omega_{\text{th}}$  for  $T = 300$  K. Also indicated is

the locus of maximizing values in the  $\lambda$ - $d$ -plane, as predicted by the approximation (63); obviously this approximation works quite well.

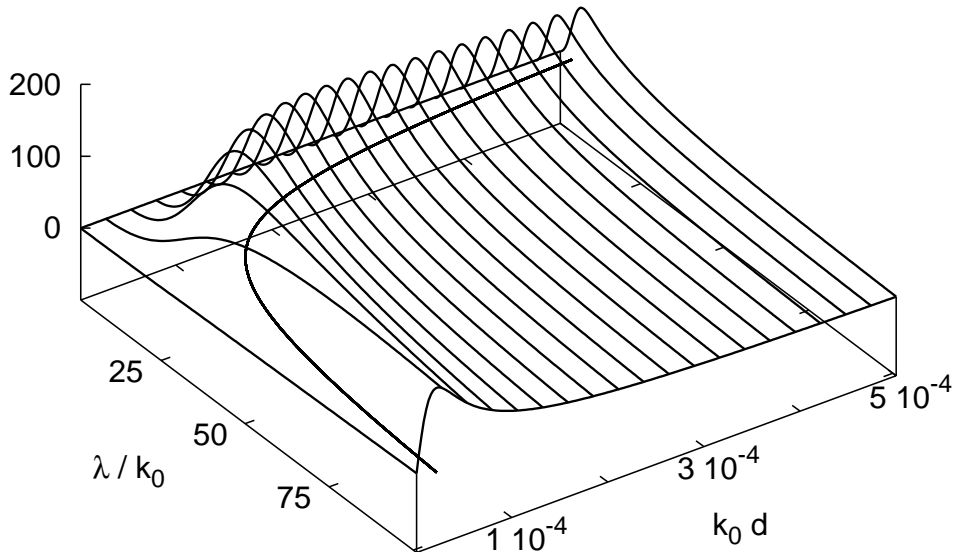


FIG. 4: Transmission function  $F(\xi)$  with  $\xi = 2h_2''d$ , as defined in Eq. (52), for evanescent TM modes, so that  $a = r_{\parallel}^2$ . The permittivity is given by the Drude formula (2) with parameters corresponding to Bismuth, as in Fig. 2; the frequency  $\omega = 10^{14} \text{ s}^{-1}$  is close to the dominant thermal frequency for  $T = 300 \text{ K}$ . The locus of the maximizing argument  $\xi_{\max}$  is well described by the approximate Eq. (63).

On the other hand, for evanescent TE modes the approximation (62) implies  $|a''| \ll |a'|$ , so that the transmission function now is cast into the different form

$$F(\xi) \approx \frac{\xi}{[1 - a'(1 - \xi)]^2}, \quad (65)$$

with its maximum located at

$$\xi_{\max} = \left| \frac{a' - 1}{a'} \right|. \quad (66)$$

This predicts

$$d_{\perp}^{\text{ev}} = \frac{1}{2h_2''} \left| \frac{\text{Re}(r_{\perp}^2) - 1}{\text{Re}(r_{\perp}^2)} \right| \quad (67)$$

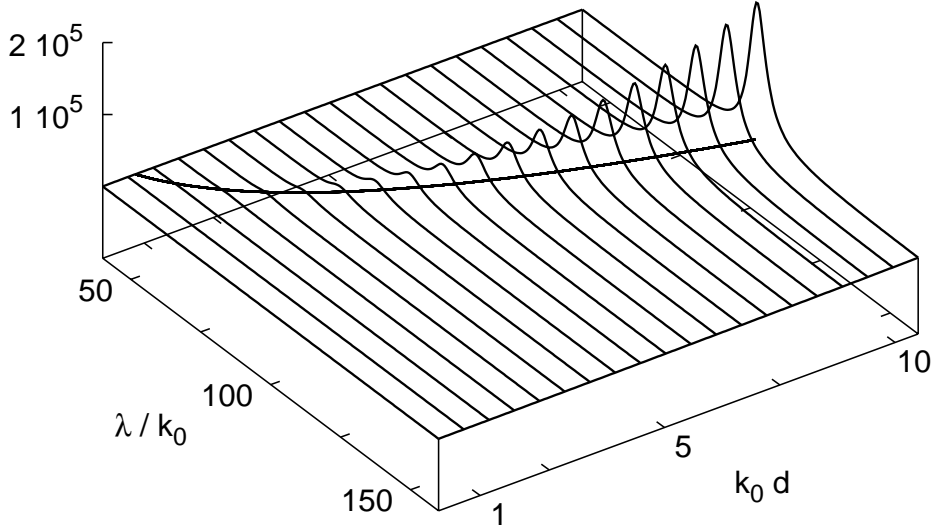


FIG. 5: Transmission function  $F(\xi)$  with  $\xi = 2h_2''d$ , as defined in Eq. (52), for evanescent TE modes, so that  $a = r_{\perp}^2$ . The permittivity is given by the Drude formula (2) with parameters corresponding to Bismuth, as in Fig. 2; the frequency  $\omega = 10^{14} \text{ s}^{-1}$  is close to the dominant thermal frequency for  $T = 300 \text{ K}$ . The locus of the maximizing argument  $\xi_{\max}$  is well described by the approximate Eq. (67). Observe how the scales here differ from those in Fig. 4.

as the optimum thickness for strongly evanescent TE modes, which simplifies to

$$k_0 d_{\perp}^{\text{ev}} \approx 8 \left( \frac{\omega}{\omega_p^2 \tau} \right)^2 \left( \frac{\lambda}{k_0} \right)^3 \quad (68)$$

in the Hagen–Rubens regime. Again, we display in Fig. 5 a plot of the function (52), and indicate the forecast of the approximation (67) for maximum transmission. Comparison of Figs. 4 and 5 reveals entirely opposite trends followed by both types of modes: Whereas for TM modes maximum transmission occurs for comparatively small  $\lambda$ , unless  $k_0 d$  is excessively low, the maximizing  $\lambda$  grows with  $k_0 d$  in the case of TE modes.

These opposite trends leave their imprints in the near-field energy density. The energy density  $\langle u^{\text{ev}} \rangle(z)$  associated with evanescent modes of either type of polarization at a distance  $z$  from the film’s surface is obtained by integrating the spectral density  $\varrho^{\text{ev}}(\omega; d, z)$

characterizing a film of thickness  $d$  in vacuum,

$$\langle u^{\text{ev}} \rangle(z) = \int_0^\infty d\omega \varrho^{\text{ev}}(\omega; d, z). \quad (69)$$

According to Eq. (43), we have

$$\varrho^{\text{ev}}(\omega; d, z) = \frac{1}{(2\pi)^2} \frac{E(\omega, \beta)}{\omega} \int_{k_0}^\infty d\lambda \lambda^3 e^{-2\gamma z} \frac{T^{\text{ev}}}{h'_3}, \quad (70)$$

with  $T^{\text{ev}} = T_\perp^{\text{ev}}$  or  $T^{\text{ev}} = T_\parallel^{\text{ev}}$  as given by Eq. (48), and  $\gamma = \sqrt{\lambda^2 - k_0^2}$ . Since Eq. (51) states  $T^{\text{ev}} = F(\xi)(2h'_3/\gamma)(1 + |r|^2)\text{Im}(r)$  for thin films, and since  $r_\parallel$  does not depend on  $\lambda$  for strongly evanescent modes, the spectral density  $\varrho_\parallel^{\text{ev}}(\omega; d, z)$  associated with TM modes is given essentially by the integrated product  $\lambda^2 e^{-2\lambda z} F(\xi)$ . Since the factor  $\lambda^2 e^{-2\lambda z}$  has a well-developed maximum at  $\lambda_{\text{max}} = 1/z$ , the spectral density is maximized if the factor  $F(\xi)$  is adapted to that maximum. In view of Eq. (64), it follows that

$$d_{\text{max}}(\omega, z) = \frac{2\omega z}{\omega_p^2 \tau} \quad (71)$$

is that film thickness which maximizes the spectral density  $\varrho_\parallel^{\text{ev}}(\omega; d, z)$  at a given distance  $z$ . This reasoning is confirmed in Fig. 6, which shows the full density  $\varrho_\parallel(\omega; d, z)$ , including the contribution from propagating modes, for  $z = 10^{-6}$  m and some representative frequencies  $\omega$ , again using the example of Bismuth. It is important to observe that this density is dominated by low frequencies in the limit of thin films; the maximizing thickness is well captured by the approximate Eq. (71). In marked contrast, the density  $\varrho_\perp(\omega; d, z)$  effectuated by TE modes is maximized at a thickness which becomes larger with decreasing frequency, as depicted in Fig. 7.

For calculating the near-field energy density  $\langle u^{\text{ev}} \rangle(z)$  we scale all wavenumbers by  $z$ , obtaining dimensionless quantities such as  $\eta \equiv \lambda z$ . The resulting integral over  $\eta$  can then be evaluated to zeroth order in the small parameter  $k_0 z$ , provided the error thus committed falls into a range of frequencies where it is suppressed by the Bose–Einstein function  $E(\omega, \beta)$ . This requirement is satisfied if  $z \ll \lambda_{\text{th}}$ , where

$$\lambda_{\text{th}} = \frac{\hbar c}{k_B T} \quad (72)$$

is the characteristic thermal wavelength at temperature  $T$ . With this proviso, we are led to

$$\begin{aligned} f &= (1 - e^{-2\eta d/z}) + |r|^2 (e^{-2\eta d/z} - e^{-4\eta d/z}) \\ g &= 0, \end{aligned} \quad (73)$$

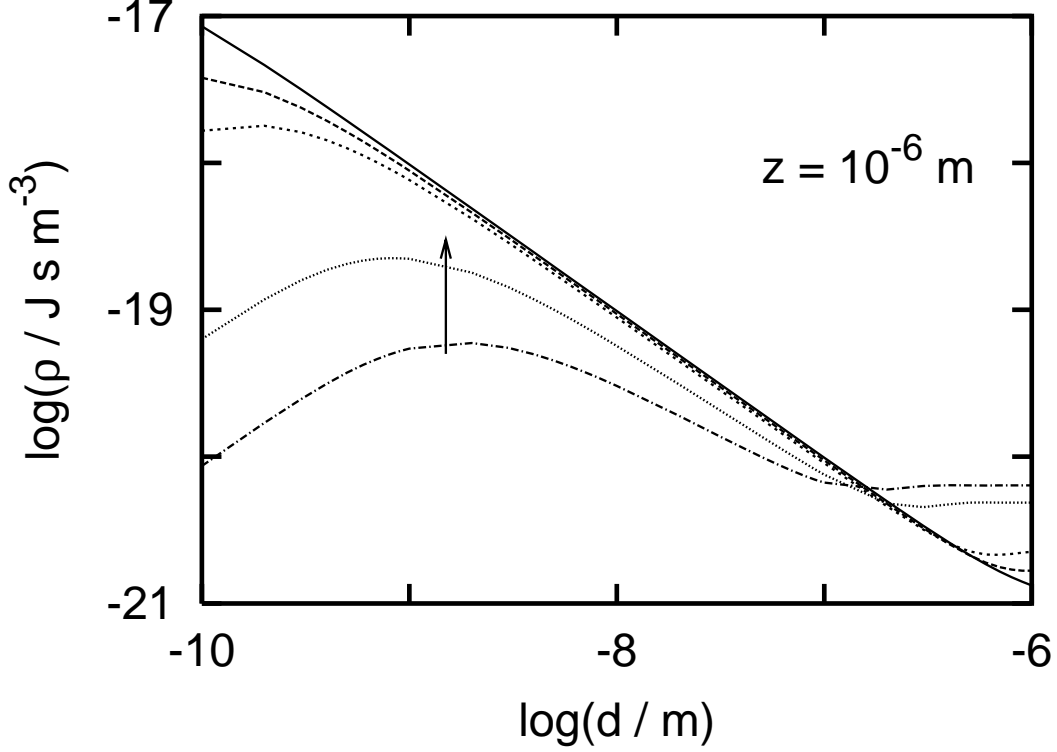


FIG. 6: Spectral density  $\varrho_{\parallel}(\omega; d, z)$  for TM modes with fixed frequency  $\omega$  originating from a metallic film at temperature  $T = 300$  K in vacuum. The density is evaluated at a distance  $z = 10^{-6}$  m from the film's surface, as function of its thickness  $d$ . The permittivity is given by the Drude formula (2) with parameters for Bismuth. The frequencies considered are  $\omega = 10^{14}$  s $^{-1}$ ,  $5 \cdot 10^{13}$  s $^{-1}$ ,  $10^{13}$  s $^{-1}$ ,  $5 \cdot 10^{12}$  s $^{-1}$ , and  $10^{12}$  s $^{-1}$ , in the direction of the arrow. The film thickness resulting in maximum density is given approximately by Eq. (71).

resulting in the near-field approximation

$$\langle u^{\text{ev}} \rangle(z) = \frac{2}{z^3} \int_0^{\infty} \frac{d\omega}{\omega} \frac{E(\omega, \beta)}{(2\pi)^2} \int_0^{\infty} d\eta \eta^2 e^{-2\eta} \frac{\text{Im}(r)}{|1 - r^2 e^{-2\eta d/z}|^2} \cdot \left[ 1 - e^{-2\eta d/z} + |r|^2 (e^{-2\eta d/z} - e^{-4\eta d/z}) \right]. \quad (74)$$

When the film thickness is still large compared to the distance from the film, so that  $z \ll d$ , this formula simplifies considerably and yields

$$\langle u^{\text{ev}} \rangle(z) = \frac{2}{z^3} \int_0^{\infty} \frac{d\omega}{\omega} \frac{E(\omega, \beta)}{(2\pi)^2} \int_0^{\infty} d\eta \eta^2 e^{-2\eta} \text{Im}(r), \quad (75)$$

which coincides with the expression for the energy density close to the surface of an infinitely thick layer, *i.e.*, of a bulk material: For distances small compared to the film thickness, the

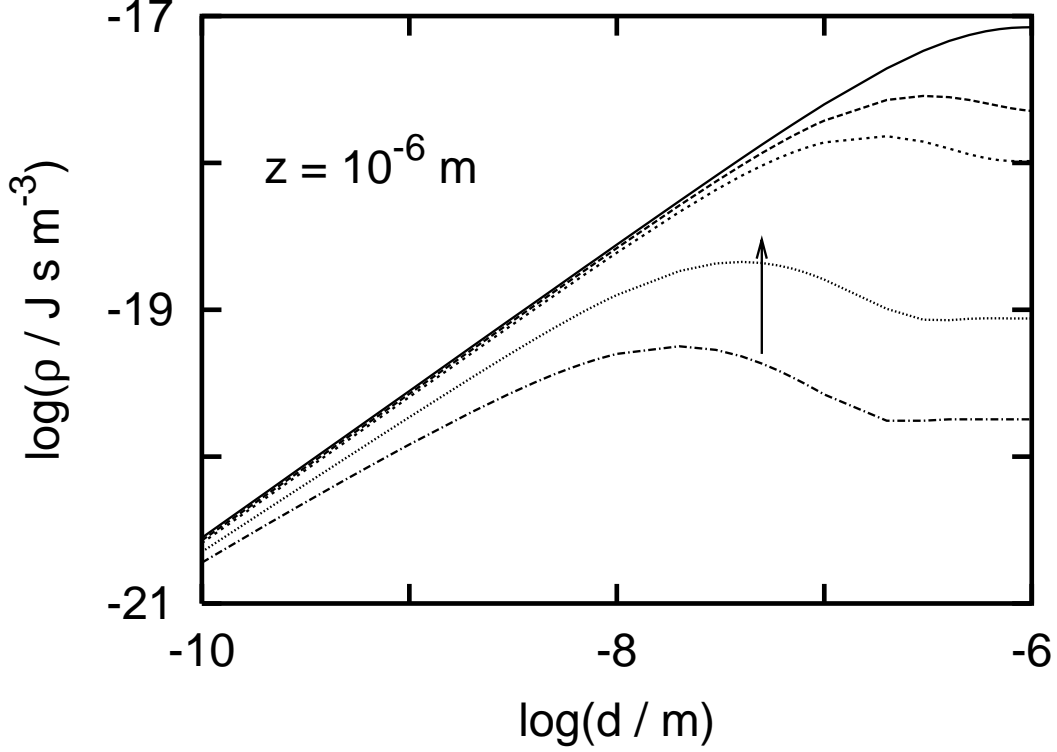


FIG. 7: Spectral density  $\varrho_{\perp}(\omega; d, z)$  for TE modes with fixed frequency  $\omega$  originating from a metallic film at temperature  $T = 300$  K in vacuum. The density is evaluated at a distance  $z = 10^{-6}$  m from the film's surface, as function of its thickness  $d$ . The permittivity is given by the Drude formula (2) with parameters for Bismuth. The frequencies considered are  $\omega = 10^{14}$  s $^{-1}$ ,  $5 \cdot 10^{13}$  s $^{-1}$ ,  $10^{13}$  s $^{-1}$ ,  $5 \cdot 10^{12}$  s $^{-1}$ , and  $10^{12}$  s $^{-1}$ , in the direction of the arrow.

energy density contains no information about that thickness. For metal films, the above result reduces to

$$\begin{aligned} \langle u_{\perp}^{\text{ev}} \rangle(z) &\approx \frac{1}{4z} \frac{1}{(2\pi c)^2} \int_0^{\infty} d\omega \omega E(\omega, \beta) \varepsilon_r'' \\ &\approx \frac{1}{96} \frac{\omega_p^2 \tau}{c^2 z} \frac{(k_B T)^2}{\hbar} \quad (z \ll d) \end{aligned} \quad (76)$$

for TE modes, and to

$$\begin{aligned} \langle u_{\parallel}^{\text{ev}} \rangle(z) &\approx \frac{1}{z^3} \int_0^{\infty} \frac{d\omega}{\omega} \frac{E(\omega, \beta)}{(2\pi)^2} \frac{\varepsilon_r''}{|\varepsilon_r + 1|^2} \\ &\approx \frac{1}{24} \frac{1}{\omega_p^2 \tau z^3} \frac{(k_B T)^2}{\hbar} \quad (z \ll d) \end{aligned} \quad (77)$$

for TM modes. In both these cases, the first expression on the respective r.h.s. is valid in general, whereas the second one requires the Hagen–Rubens approximation. Thus, for rather

short distances  $z \ll d$  the total energy density is dominated by the TM modes, exhibiting the familiar  $z^{-3}$ -divergence known from bulk materials [7, 31].

In contrast, the other limiting case of distances large compared to the film thickness,  $d \ll z \ll \lambda_{\text{th}}$ , gives rise to a fairly counterintuitive feature. The general expression (74) then takes the form

$$\begin{aligned} \langle u^{\text{ev}} \rangle(z) &= \frac{2}{z^3} \int_0^\infty \frac{d\omega}{\omega} \frac{E(\omega, \beta)}{(2\pi)^2} \int_0^\infty d\eta \eta^2 e^{-2\eta} \frac{\text{Im}(r)}{|1 - r^2(1 - 2\eta d/z)|^2} \\ &\quad \cdot 2\eta \frac{d}{z} (1 + |r|^2) . \end{aligned} \quad (78)$$

For TE modes, Eq. (61) guarantees that the denominator appearing here may be replaced by unity. This simplification then gives

$$\begin{aligned} \langle u_{\perp}^{\text{ev}} \rangle(z) &\approx \frac{1}{4z^2} \frac{d}{(2\pi c)^2} \int_0^\infty d\omega \omega E(\omega, \beta) \varepsilon_r'' \\ &\approx \frac{1}{96} \frac{\omega_p^2 \tau d (k_B T)^2}{c^2 z^2 \hbar} \quad (d \ll z \ll \lambda_{\text{th}}) , \end{aligned} \quad (79)$$

where once again the second approximate equality hinges on the Hagen–Rubens condition. Observe that this result differs from the previous Eq. (76) for the reverse situation only by the factor  $d/z \ll 1$ , which appears reasonable: The energy density caused by TE modes at a fixed distance  $z \ll \lambda_{\text{th}}$  decreases when reducing the film thickness.

However, the situation is more delicate when dealing with TM modes, for which Eq. (60) enforces  $\text{Re}(r_{\parallel}^2) \approx 1$  and  $|\text{Im}(r_{\parallel}^2)| \ll 1$ , so that the integrand in Eq. (78) acquires a small denominator. We still may write

$$|1 - r_{\parallel}^2(1 - 2\eta d/z)|^2 \approx |2\eta d/z - i \text{Im}(r_{\parallel}^2)|^2 , \quad (80)$$

and now have to make a further distinction: Keeping in mind that the decisive  $\eta$  are on the order of unity, we may set

$$|1 - r_{\parallel}^2(1 - 2\eta d/z)|^2 \approx (2\eta d/z)^2 , \quad (81)$$

provided  $2d/z \gg \text{Im}(r_{\parallel}^2)$  for all relevant frequencies  $\omega \lesssim k_B T/\hbar$ . In view of Eq. (60), this requires

$$\frac{d}{z} \gg \frac{2k_B T}{\hbar \omega_p^2 \tau} . \quad (82)$$



It is interesting to observe that this condition validating the approximation (81) can be cast into a particularly suggestive form involving only the Woltersdorff thickness (56) and the characteristic thermal wavelength (72):

$$\frac{d}{z} \gg \frac{d_W}{\lambda_{\text{th}}} ; \quad (83)$$

in terms of the maximizing thickness (71), this means nothing but

$$d \gg d_{\text{max}}(k_B T / \hbar, z) . \quad (84)$$

Given this, we find

$$\begin{aligned} \langle u_{\parallel}^{\text{ev}} \rangle(z) &\approx \frac{1}{dz^2} \int_0^{\infty} \frac{d\omega}{\omega} \frac{E(\omega, \beta)}{(2\pi)^2} \frac{\varepsilon_r''}{|\varepsilon_r + 1|^2} \\ &\approx \frac{1}{24} \frac{1}{\omega_p^2 \tau dz^2} \frac{(k_B T)^2}{\hbar} \quad (d_{\text{max}}(k_B T / \hbar, z) \ll d \ll z) \end{aligned} \quad (85)$$

for films which are not too thin. This expression differs from its counterpart (77) by the factor  $z/d \gg 1$ , which is noteworthy: In the near-field regime, the energy density caused by TM modes increases substantially when reducing the thickness of the film, despite the loss of source volume. The fact that this feature emerges only for the TM modes indicates that it is related to surface plasmon polaritons. Indeed, when the film thickness  $d$  is sufficiently small, the plasmons associated with the two surfaces couple, splitting into one resonance with a frequency that converges to  $\omega_p$  for  $d \rightarrow 0$ , and a second resonance with a frequency that approaches zero [19, 32]. This is exemplified in Fig. 8, where we plot the local density of states  $D_{\parallel}(\omega, d, z)$ , defined through the relation [6]

$$\langle u_{\parallel}^{\text{ev}}(z) \rangle = \int_0^{\infty} d\omega E(\omega, \beta) D_{\parallel}(\omega, d, z) , \quad (86)$$

for a distance of  $z = 10^{-8}$  m from Bismuth films of various thicknesses. The increase of the energy density  $\langle u_{\parallel}^{\text{ev}} \rangle(z)$  with decreasing film thickness found in Eq. (85) occurs when the low-frequency surface plasmon polariton comes into the range of the thermal frequencies.

Our findings are illustrated in Fig. 9, which shows the individual densities  $\langle u_{\perp}(z) \rangle$  and  $\langle u_{\parallel}(z) \rangle$  at a distance  $z = 10^{-6}$  m from the surface of a Bismuth film, together with their sum, again as functions of the film thickness  $d$ . Whereas the density caused by TE modes decreases monotonically with decreasing  $d$ , the one associated with TM modes actually increases, and approaches a finite value for  $d \rightarrow 0$ . These different trends obeyed by the two

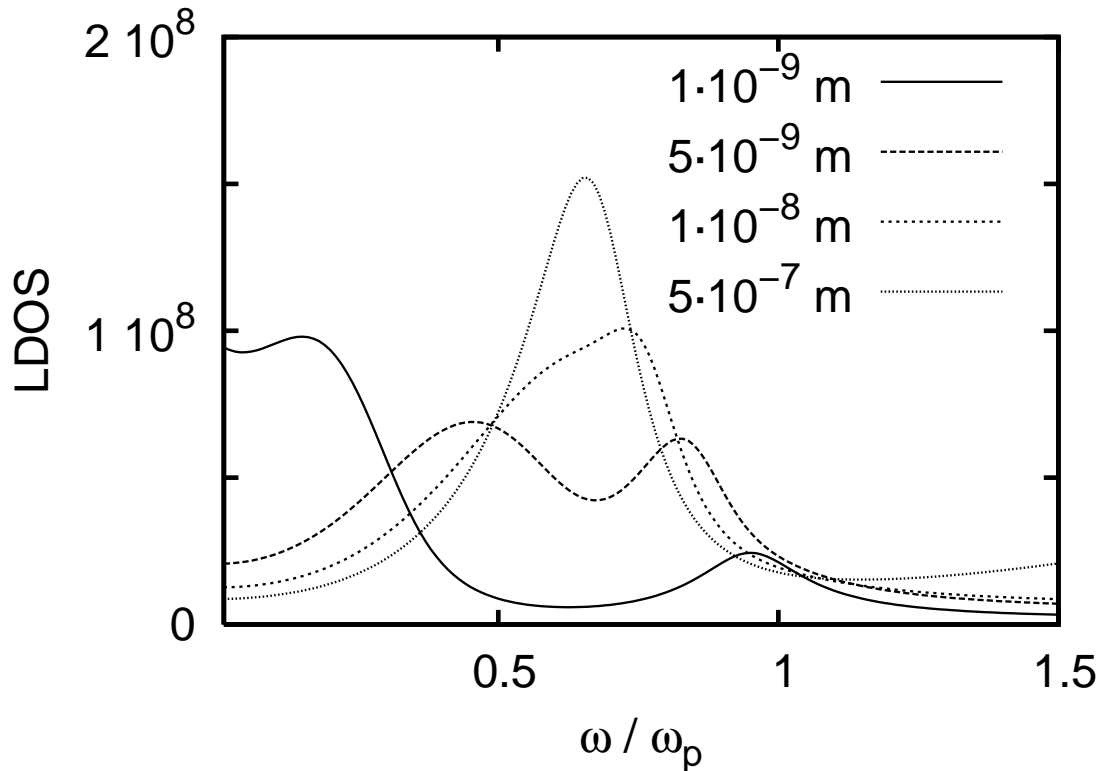


FIG. 8: Local density of states  $D_{\parallel}(\omega, d, z)$  at distance  $z = 10^{-8}$  m above a Bismuth film of thickness  $d$ , specified by the line style. For  $d = 5 \cdot 10^{-7}$  m, one observes the usual surface plasmon polariton resonance at  $\omega = \omega_p/\sqrt{2}$ . For lower  $d$ , the resonances associated with the two surfaces of the film couple and split. The higher resonance approaches  $\omega_p$  for vanishing film thickness, whereas the lower one approaches  $\omega = 0$ . This latter, low-frequency resonance causes the universal behavior expressed in Eq. (93).

types of modes result in a non-monotonic dependence of the total energy density at  $z$  on the thickness  $d$ .

The limiting case of very thin films is reached when  $d/z \ll d_W/\lambda_{\text{th}}$ , or

$$d \ll d_{\text{max}}(k_B T/\hbar, z). \quad (87)$$

This limit may be hard to realize in practice, and fall outside the regime of validity of macroscopic electrodynamics for most materials, but it is nonetheless of conceptual interest.

It necessitates to approximate the denominator in the expression (78) in the form

$$\left| 1 - r_{\parallel}^2 \left( 1 - 2\eta \frac{d}{z} \right) \right|^2 \approx \left( 2\eta \frac{d}{z} \right)^2 + \left( \frac{4\omega}{\omega_p^2 \tau} \right)^2, \quad (88)$$

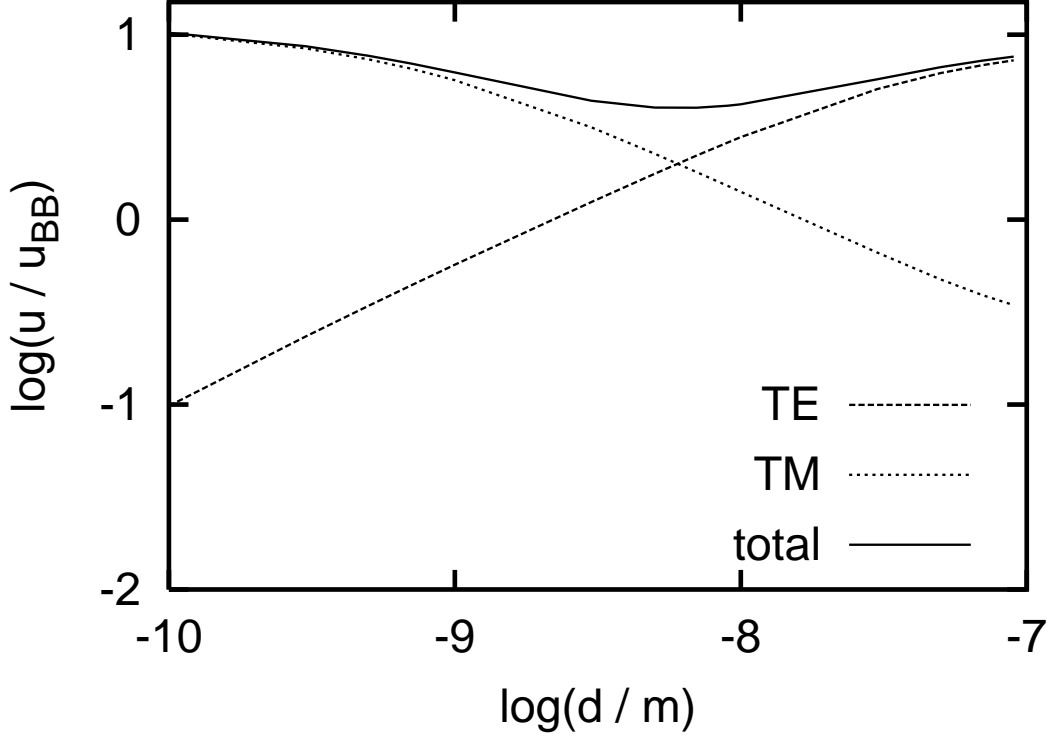


FIG. 9: Total energy density  $\langle u(z) \rangle = \langle u_{\perp}(z) \rangle + \langle u_{\parallel}(z) \rangle$ , together with the individual contributions, at a distance  $z = 10^{-6}$  m from the surface of a Drude metal film with thickness  $d$ . The Drude parameters correspond to Bismuth; the temperature is  $T = 300$  K. Data are normalized with respect to the energy density  $u_{\text{BB}}$  of a black body of the same temperature.

with none of the two terms on the r.h.s. being negligible against the other for all relevant frequencies. Inserting, one is confronted with

$$\begin{aligned} \langle u_{\parallel}^{\text{ev}} \rangle(z) &\approx \frac{2}{z^3} \int_0^{\infty} \frac{d\omega}{\omega} \frac{E(\omega, \beta)}{(2\pi)^2} \int_0^{\infty} d\eta \eta^2 e^{-2\eta} \frac{\text{Im}(r_{\parallel})}{|2\eta d/z - i \text{Im}(r_{\parallel}^2)|^2} 4\eta d/z \\ &\approx \frac{2}{z^2 d} \frac{2}{\omega_p^2 \tau} \int_0^{\infty} d\omega \frac{E(\omega, \beta)}{(2\pi)^2} \int_0^{\infty} d\eta \eta^3 \frac{e^{-2\eta}}{\eta^2 + \left(\frac{2\omega z}{\omega_p^2 \tau d}\right)^2}. \end{aligned} \quad (89)$$

Rescaling the  $\eta$ -integral according to

$$\int_0^{\infty} d\eta \frac{\eta^3 e^{-2\eta}}{\eta^2 + a^2} = a^2 \int_0^{\infty} dy \frac{y^3 e^{-2ay}}{y^2 + 1}, \quad (90)$$

we arrive at

$$\langle u_{\parallel}^{\text{ev}} \rangle(z) \approx \frac{1}{\pi^2 z^2 \omega_p^2 \tau d} \int_0^{\infty} d\omega E(\omega, \beta) \left(\frac{2\omega z}{\omega_p^2 \tau d}\right)^2 \int_0^{\infty} dy \frac{y^3 \exp\left(-2y \frac{2\omega z}{\omega_p^2 \tau d}\right)}{y^2 + 1}. \quad (91)$$

Clearly, here the  $\omega$ -integral is dominated by low frequencies in the small- $d$ -limit, as discussed before in the context of Fig. 6; consequently, we are entitled to replace  $E(\omega, \beta)$  by  $k_B T$ . Then interchanging the order of integration, and using

$$\int_0^\infty d\omega \left( \frac{2\omega z}{\omega_p^2 \tau d} \right)^2 \exp \left( -2y \frac{2\omega z}{\omega_p^2 \tau d} \right) = \frac{\omega_p^2 \tau d}{z} \frac{1}{(2y)^3}, \quad (92)$$

finally results in

$$\begin{aligned} \langle u_{\parallel}^{\text{ev}} \rangle(z) &\approx \frac{k_B T}{\pi^2 z^3} \frac{1}{2^3} \int_0^\infty \frac{dy}{y^2 + 1} \\ &= \frac{k_B T}{16\pi z^3} \quad (d \ll d_{\text{max}}(k_B T/\hbar, z)). \end{aligned} \quad (93)$$

Remarkably, the energy density associated with evanescent TM modes not only remains finite when approaching the (formal) limit of zero thickness, but it also becomes independent of the metal's parameters. This universal feature stems from the fact that the low-frequency surface plasmon polariton resonance depicted in Fig. 8 converges to zero frequency for all Drude materials. Nonetheless, the width of this resonance depends on the relaxation time  $\tau$ , so that the scale  $d_{\text{max}}$  below which the universal behavior appears is proportional to  $1/\tau$ . As a consequence, metals such as gold and Bismuth, which possess nearly identical plasma frequencies but substantially different relaxation times, reveal the above universality for rather different film thicknesses. As will be discussed in Ref. [27], the rise of the evanescent energy density expressed by Eqs. (85) and (93) also occurs with thin metal films coating a polar dielectric, but is lost when a thin metal film covers another metal.

Figure 10 shows a doubly logarithmic plot of the dependence of the energy density  $\langle u_{\perp}(z) \rangle$  associated with TE modes on the distance  $z$  from the film, summing up evanescent and propagating contributions. Again we take Drude parameters for Bismuth at temperature  $T = 300$  K, and consider films of thickness  $d = 10^{-7}$  m and  $7 \cdot 10^{-9}$  m, together with an excessively thin model example with  $d = 10^{-10}$  m. In the first two cases, one clearly recognizes the crossover from the  $z^{-1}$ -behavior predicted for  $z \ll d$  by the approximation (76) to the  $z^{-2}$ -dependence implied by Eq. (79) for larger distances,  $d \ll z \ll \lambda_{\text{th}}$ . As indicated by the arrow,  $\langle u_{\perp}(z) \rangle$  decreases at fixed  $z$  when  $d$  is reduced.

Figure 11 displays the corresponding plot for TM modes. Here the data for  $d = 10^{-7}$  m and  $d = 7 \cdot 10^{-9}$  m exhibit the change of slope from  $-3$ , as deduced from Eq. (77) for  $z \ll d$ , to  $-2$ , as required by Eq. (85) for  $d \ll z \ll \lambda_{\text{th}}$ . Moreover, for the model case  $d = 10^{-10}$  m

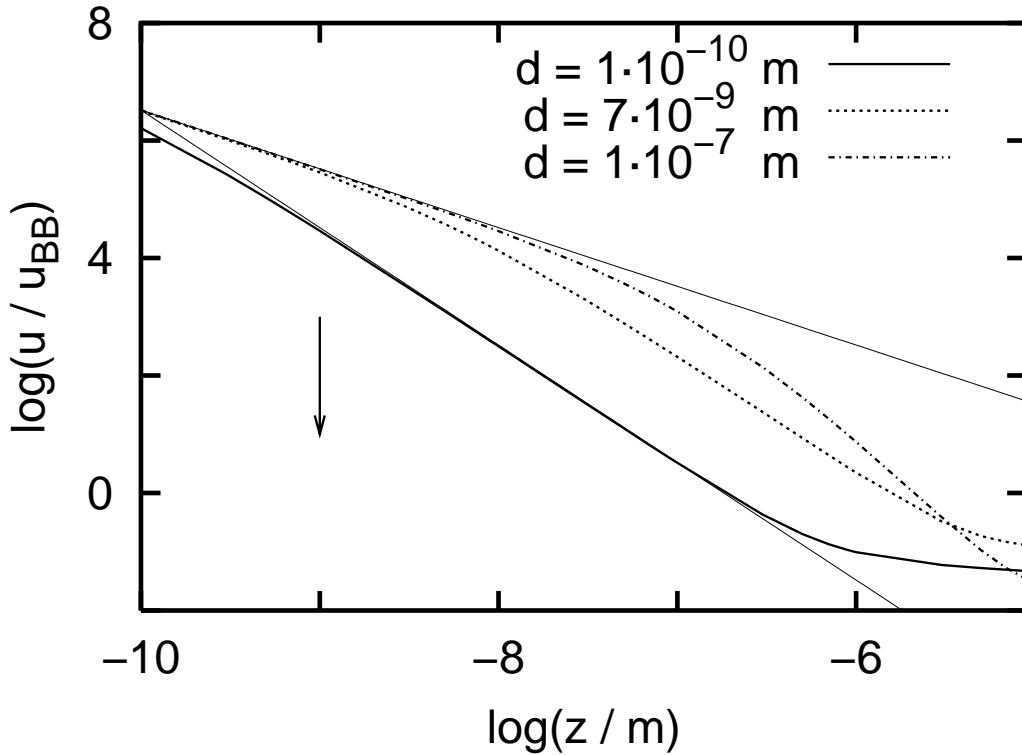


FIG. 10: Energy density  $\langle u_{\perp}(z) \rangle$  associated with TE modes for Drude metal films with Bismuth parameters at  $T = 300 \text{ K}$ , as functions of the distance  $z$  from the film. Film thicknesses are  $d = 10^{-7} \text{ m}$  (dashed-dotted),  $7 \cdot 10^{-9} \text{ m}$  (dotted), and  $10^{-10} \text{ m}$  (full line). For fixed  $z$  in the near-field regime, this density  $\langle u_{\perp}(z) \rangle$  decreases with decreasing thickness. Straight lines correspond to the approximate results (76) and (79) for the thickest and thinnest film, respectively. Data are normalized with respect to the energy density  $u_{\text{BB}}$  of a black body of the same temperature.

one observes another crossover from that slope  $-2$  appearing when  $d_{\text{max}}(k_{\text{B}}T/\hbar, z) \ll d$  to the universal  $z^{-3}$ -behavior found in Eq. (93) in the opposite limit.

Finally, we display in Fig. 12 the total energy densities for these examples. As a consequence of the opposing trends obeyed by the TE and TM modes, there is a well-developed range of distances around  $z \approx 10^{-7} \text{ m}$  where the total density varies non-monotonically with the film thickness.

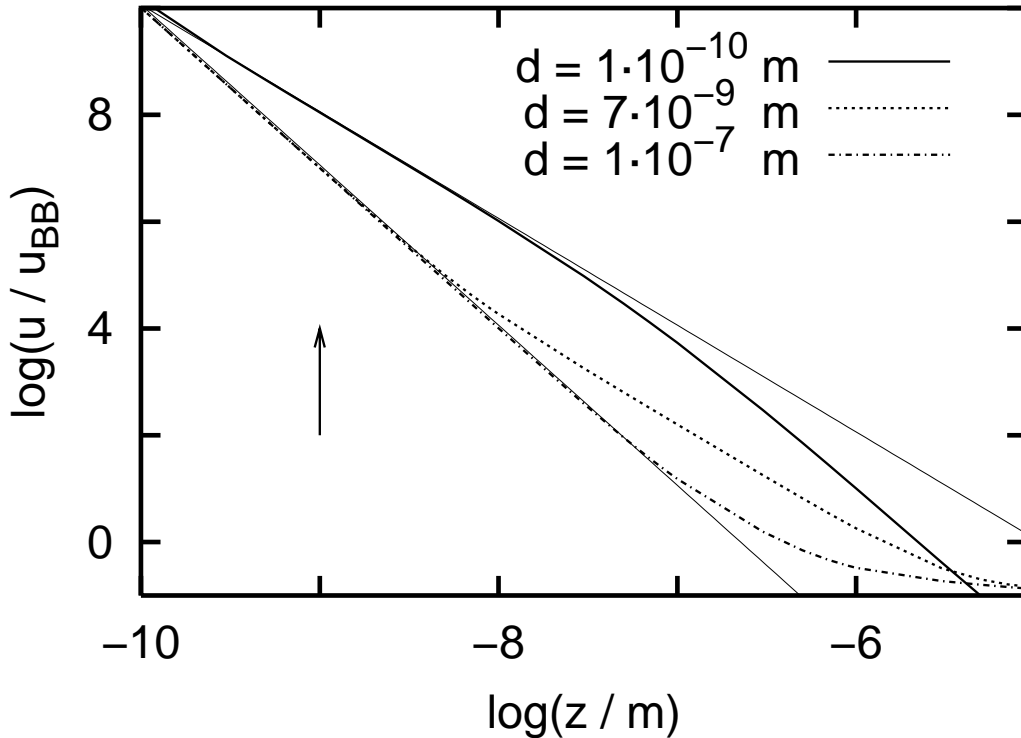


FIG. 11: Energy density  $\langle u_{\parallel}(z) \rangle$  associated with TM modes for Drude metal films with Bismuth parameters at  $T = 300$  K, as functions of the distance  $z$  from the film. Line symbols are as in Fig. 10. For fixed  $z$ , the density  $\langle u_{\parallel}(z) \rangle$  increases with decreasing thickness. Straight lines correspond to the approximate results (77) and (85) for the thickest and thinnest film, respectively.

## VI. CONCLUSIONS

A theoretical treatment of heat radiation and thermal near fields generated by thin dielectric slabs within the framework of macroscopic fluctuational electrodynamics hinges on two basic ingredients. On the one hand, Maxwell's equations have to be solved with the boundary conditions imposed by the slab geometry; on the other, the dielectric permittivity  $\varepsilon(\omega)$  for the slab's material is required. We have addressed the first problem by constructing the dyadic Green's functions for the slab in Sec. III, and stated general expressions for both the intensity of the heat radiation and its energy density, valid for any prescribed permittivity  $\varepsilon(\omega)$ , in Sec. IV.

The restriction to metallic films, with dielectric response solely due to free particle-like electron motion, leads to an intricate competition of length scales. Besides the geometrical

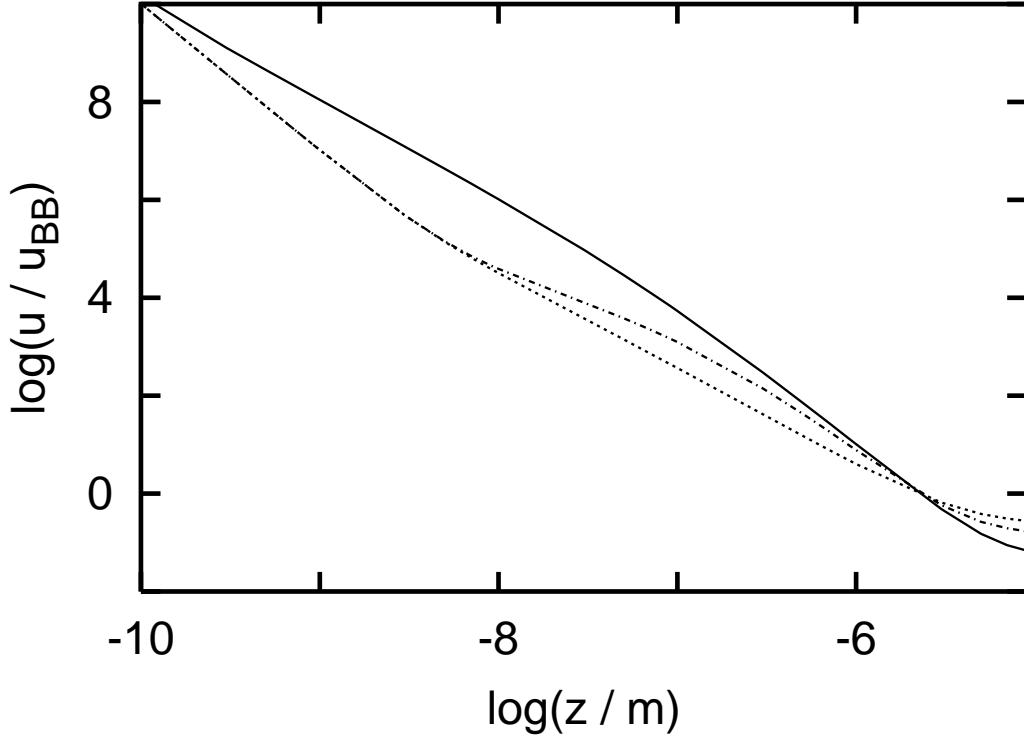


FIG. 12: Total energy density  $\langle u(z) \rangle = \langle u_{\perp}(z) \rangle + \langle u_{\parallel}(z) \rangle$ , for the same example cases as studied in Figs. 10 and 11. Observe that the energy density varies non-monotonically with film thickness for distances around  $z \approx 10^{-7}$  m.

thickness  $d$  of such a film, and the skin depth (1), the Woltersdorff thickness  $d_{\text{W}}$  defined in Eq. (56) and the characteristic thermal wavelength  $\lambda_{\text{th}}$  come into play. As a consequence, the dependence of the thermal near-field energy density on the distance  $z$  from the film's surface is not characterized by a single exponent, but different exponents dominate in different regimes. In particular, we have shown that for  $d/z \ll d_{\text{W}}/\lambda_{\text{th}}$  the energy density is dominated by the universal contribution (93) brought about by TM modes. Our conclusions are based on the Drude model (2) for the permittivity, regarding the plasma frequency  $\omega_{\text{p}}$  and the relaxation time  $\tau$  as fixed. This does not hold exactly for electrical transport in ultrathin metallic films, since the resistivity of such a film increases with decreasing thickness [33], but we expect the main features of our discussion to persist at least qualitatively.

With a view towards laboratory experiments, one might be interested not in metallic films in vacuum, but rather in thin metal coatings on a planar surface of another material. This case has been anticipated in our general formulae (47) and (48), where the Fresnel reflection

coefficients for the left interface differ from those for the right one, but one still has to account for the bulk contribution [26, 27]. Qualitatively, however, the Fabry–Perot-like effect brought about by thin metal coatings bears interesting possibilities of manipulating the intensity of thermal radiation, that is, the amount of energy transported per time from a hot body into the vacuum.

The insights obtained in this work are especially pertinent with regard to recent developments in scanning thermal microscopy [34, 35]. It has been argued that the tip of a thermal microscope operating in ultrahigh vacuum is sensitive to the near-field energy density above the sample; experiments along this direction are presently underway [36]. Near-field signatures offered by thin films, or by bulk materials coated with films of varying, exactly specified thickness even down to that of atomic monolayers, and their actual observation in a suitable experiment could be of value for developing scanning thermal microscopy into a quantitative tool for materials science.

While we have formally extrapolated the realm of macroscopic electrodynamics down to even unrealistically small scales, it goes without saying that at some scale deviations from the macroscopic description will show up; such deviations now have come within the scope of modern experimental set-ups [36]. In addition, one has to expect important corrections due to effects of non-local optical response [31, 37]. The pursuit of the question at precisely what length scale, and in precisely what manner, these deviations start to manifest themselves is a quite important task in nanoscale thermal engineering. In this quest, the present study may serve as a reference.

## **Acknowledgments**

S.-A. B. acknowledges support from the Studienstiftung des deutschen Volkes. We thank U. Fleischmann-Wischnath, O. Huth, A. Kittel, A. Knübel, J. Parisi, and F. Rütting for helpful discussions and criticism.

## **Appendix A: Calculation of the Poynting vector**

In this Appendix we provide technical details required for the derivation of the expression (32) for the intensity of heat radiation emitted by a dielectric layer. Computing the



magnetic Green's function  $\mathbb{G}_{IV}^H$  according to Eq. (14) from the electric Green's function (26), and defining the convenient symbols

$$\begin{aligned}
a_{\perp}^{ij} &:= h_i + h_j \\
a_{\parallel}^{ij} &:= h_i \frac{\varepsilon_j}{\varepsilon_i} + h_j \\
b_{\perp}^{ij} &:= h_i - h_j \\
b_{\parallel}^{ij} &:= h_i \frac{\varepsilon_j}{\varepsilon_i} - h_j,
\end{aligned} \tag{A1}$$

one starts from the product of the two dyadics and integrates, obtaining

$$\begin{aligned}
\int d^3 r' \mathbb{G}_{IV}^E \cdot \overline{\mathbb{G}_{IV}^H}^t &= \frac{i}{(2\pi)^2 \omega \mu_0} \int_0^\infty d\lambda \int_0^\infty d\lambda' \sum_{n,n'=0}^\infty \frac{(2 - \delta_{n,0})(2 - \delta_{n',0})}{\lambda \lambda'} \left\{ \right. \\
&\frac{\overline{k_3}}{|D_{\perp}|^2} \mathbf{M}(h_3) \otimes \overline{\mathbf{N}}(h_3) \cdot \\
&\left[ |a_{\perp}^{12}|^2 e^{2h_2'' d} I_{\mathbf{M}}^{--} - a_{\perp}^{12} \overline{b_{\perp}^{12}} e^{-2ih_2' d} I_{\mathbf{M}}^{-+} - b_{\perp}^{12} \overline{a_{\perp}^{12}} e^{2ih_2' d} I_{\mathbf{M}}^{+-} + |b_{\perp}^{12}|^2 e^{-2h_2'' d} I_{\mathbf{M}}^{++} \right] \\
&+ \frac{|k_2|^2}{|D_{\parallel}|^2 k_3} \mathbf{N}(h_3) \otimes \overline{\mathbf{M}}(h_3) \cdot \\
&\left. \left[ |a_{\parallel}^{12}|^2 e^{2h_2'' d} I_{\mathbf{N}}^{--} - a_{\parallel}^{12} \overline{b_{\parallel}^{12}} e^{-2ih_2' d} I_{\mathbf{N}}^{-+} - b_{\parallel}^{12} \overline{a_{\parallel}^{12}} e^{2ih_2' d} I_{\mathbf{N}}^{+-} + |b_{\parallel}^{12}|^2 e^{-2h_2'' d} I_{\mathbf{N}}^{++} \right] \right\}. \tag{A2}
\end{aligned}$$

Here we have introduced the source integrals

$$\begin{aligned}
I_{\mathbf{M}}^{--} &:= \int d^3 r' \mathbf{M}'(-h_2) \cdot \overline{\mathbf{M}}'(-h_2) = \Delta_{n,n'}^{\lambda,\lambda'} \frac{1}{h_2''} (1 - e^{-2h_2'' d}) \\
I_{\mathbf{M}}^{-+} &:= \int d^3 r' \mathbf{M}'(-h_2) \cdot \overline{\mathbf{M}}'(h_2) = \Delta_{n,n'}^{\lambda,\lambda'} \frac{1}{ih_2'} (e^{2ih_2' d} - 1) \\
I_{\mathbf{M}}^{+-} &:= \int d^3 r' \mathbf{M}'(h_2) \cdot \overline{\mathbf{M}}'(-h_2) = \Delta_{n,n'}^{\lambda,\lambda'} \frac{1}{ih_2'} (1 - e^{-2ih_2' d}) \\
I_{\mathbf{M}}^{++} &:= \int d^3 r' \mathbf{M}'(h_2) \cdot \overline{\mathbf{M}}'(h_2) = \Delta_{n,n'}^{\lambda,\lambda'} \frac{1}{h_2''} (e^{2h_2'' d} - 1),
\end{aligned} \tag{A3}$$

where the integration extends over the dielectric layer labeled “2”, that is, over the slab  $-d \leq z \leq 0$  occupied by the sources (cf. Fig. 1); the symbol  $\Delta_{n,n'}^{\lambda,\lambda'}$  is given by

$$\Delta_{n,n'}^{\lambda,\lambda'} := \frac{1 + \delta_{n,0}}{2} \delta_{n,n'} \pi \lambda \delta(\lambda - \lambda'). \tag{A4}$$

Likewise, one has

$$\begin{aligned}
I_{\mathbf{N}}^{-} &:= \int d^3 r' \mathbf{N}'(-h_2) \cdot \overline{\mathbf{N}}'(-h_2) = \Delta_{n,n'}^{\lambda,\lambda'} \frac{\lambda^2 + |h_2|^2}{|k_2|^2} \frac{1}{h_2''} (1 - e^{-2h_2''d}) \\
I_{\mathbf{N}}^{-+} &:= \int d^3 r' \mathbf{N}'(-h_2) \cdot \overline{\mathbf{N}}'(h_2) = \Delta_{n,n'}^{\lambda,\lambda'} \frac{\lambda^2 - |h_2|^2}{|k_2|^2} \frac{1}{ih_2'} (e^{2ih_2'd} - 1) \\
I_{\mathbf{N}}^{+-} &:= \int d^3 r' \mathbf{N}'(+h_2) \cdot \overline{\mathbf{N}}'(-h_2) = \Delta_{n,n'}^{\lambda,\lambda'} \frac{\lambda^2 - |h_2|^2}{|k_2|^2} \frac{1}{ih_2'} (1 - e^{-2ih_2'd}) \\
I_{\mathbf{N}}^{++} &:= \int d^3 r' \mathbf{N}'(+h_2) \cdot \overline{\mathbf{N}}'(h_2) = \Delta_{n,n'}^{\lambda,\lambda'} \frac{\lambda^2 + |h_2|^2}{|k_2|^2} \frac{1}{h_2''} (e^{2h_2''d} - 1). \quad (\text{A5})
\end{aligned}$$

The emergence of the 8 different source integrals (A3) and (A5) is a characteristic complication brought about by the finite thickness of the slab; it can be seen as a consequence of multiple reflections inside the slab. Inserting the right hand sides of these integrals, the longish expression (A2) is reduced to

$$\begin{aligned}
\int d^3 r' \mathbf{G}_{IV}^E \cdot \overline{\mathbf{G}}_{IV}^{H^t} &= \frac{i}{4\pi\omega\mu_0} \int_0^\infty d\lambda \sum_{n=0}^\infty \frac{2 - \delta_{n,0}}{\lambda} \left\{ \right. \\
&\quad \frac{\overline{k}_3}{|D_\perp|^2} \left[ \frac{1}{h_2''} A_\perp + \frac{1}{h_2'} B_\perp \right] \mathbf{M}(h_3) \otimes \overline{\mathbf{N}}(h_3) \\
&\quad \left. + \frac{|k_2|^2}{|D_\parallel|^2 k_3} \left[ \frac{A_\parallel}{h_2''} \frac{\lambda^2 + |h_2|^2}{|k_2|^2} + \frac{B_\parallel}{h_2'} \frac{\lambda^2 - |h_2|^2}{|k_2|^2} \right] \mathbf{N}(h_3) \otimes \overline{\mathbf{M}}(h_3) \right\}. \quad (\text{A6})
\end{aligned}$$

In the next step, we evaluate the vector product appearing in the definition of the Poynting vector (31). Because of translational invariance in the planes orthogonal to the  $z$ -axis, it suffices to consider  $\rho = 0$  only. With the help of

$$\epsilon_{z\beta\gamma} (\mathbf{M}(h_3) \otimes \overline{\mathbf{N}}(h_3))_{\beta\gamma} \Big|_{\rho=0} = -i \frac{\overline{h}_3 \lambda^2}{2\overline{k}_3} e^{-2h_3''z} (\delta_{n,1} + \delta_{n,-1}) \quad (\text{A7})$$

and

$$\epsilon_{z\beta\gamma} (\mathbf{N}(h_3) \otimes \overline{\mathbf{M}}(h_3))_{\beta\gamma} \Big|_{\rho=0} = -i \frac{h_3 \lambda^2}{2k_3} e^{-2h_3''z} (\delta_{n,1} + \delta_{n,-1}), \quad (\text{A8})$$

and exploiting the elementary but important relations

$$\begin{aligned}
\lambda^2 + |h_2|^2 &= \frac{\text{Re}(h_2 \overline{\epsilon}_{r2}) k_0^2}{h_2'} \\
\lambda^2 - |h_2|^2 &= \frac{\text{Im}(h_2 \overline{\epsilon}_{r2}) k_0^2}{h_2''}, \quad (\text{A9})
\end{aligned}$$

where  $k_0 = \omega/c$ , one is led to

$$\begin{aligned}
\epsilon_{z\beta\gamma} \left( \int d^3 r' \mathbf{G}_{IV}^E \cdot \overline{\mathbf{G}}_{IV}^{H^t} \right)_{\beta\gamma} \Big|_{\rho=0} &= \frac{1}{4\pi\omega\mu_0} \int_0^\infty d\lambda \lambda e^{-2h_3''z} \left\{ \frac{\overline{h}_3}{|D_\perp|^2} \left[ \frac{1}{h_2''} A_\perp + \frac{1}{h_2'} B_\perp \right] \right. \\
&\quad \left. + \frac{h_3}{|D_\parallel|^2 \epsilon_{r3}} \left[ \frac{\text{Re}(h_2 \overline{\epsilon}_{r2})}{h_2' h_2''} A_\parallel + \frac{\text{Im}(h_2 \overline{\epsilon}_{r2})}{h_2' h_2''} B_\parallel \right] \right\}, \quad (\text{A10})
\end{aligned}$$

with the symbols  $A_{\perp}$ ,  $A_{\parallel}$ ,  $B_{\perp}$ , and  $B_{\parallel}$  as specified in Eqs. (35) and (36). Inserting this expression (A10) into Eq. (31), adding the complex conjugate, and utilizing the identity

$$\varepsilon_2''(\omega) = \frac{2h_2'h_2''}{\mu_0\omega^2} \quad (\text{A11})$$

for the imaginary part of the permittivity, one finally ends up with the result stated in Eq. (32).

- 
- [1] K. Joulain, J.-P. Mulet, F. Marquier, R. Carminati, and J.-J. Greffet, *Surface Science Reports* **57**, 59 (2005).
  - [2] R. Carminati and J.-J. Greffet, *Phys. Rev. Lett.* **82**, 1660 (1999).
  - [3] A. V. Shchegrov, K. Joulain, R. Carminati, and J.-J. Greffet, *Phys. Rev. Lett.* **85**, 1548 (2000).
  - [4] F. Marquier, K. Joulain, J.-P. Mulet, R. Carminati, and J.-J. Greffet, *Phys. Rev. B* **69**, 155412 (2004).
  - [5] D. Polder and M. van Hove, *Phys. Rev. B* **4**, 3303 (1971).
  - [6] K. Joulain, R. Carminati, J.-P. Mulet, and J.-J. Greffet, *Phys. Rev. B* **68**, 245405 (2003).
  - [7] S. M. Rytov, Y. A. Kravtsov, and V. I. Tatarskii, *Principles of Statistical Radiophysics*, Vol. 3 (Springer, New York, 1989).
  - [8] G. S. Agarwal, *Phys. Rev. A* **11**, 230 (1975).
  - [9] O. G. Kollyukh, A. I. Liptuga, V. O. Morozhenko, and V. I. Pipa, *Semiconductor Physics, Quantum Electronics & Optoelectronics* **6**, 210 (2003).
  - [10] A. Narayanaswamy and G. Chen, *Appl. Phys. Lett.* **82**, 3544 (2003).
  - [11] B. W. Ninham and V. A. Parsegian, *J. Chem. Phys.* **52**, 4578 (1970).
  - [12] B. W. Ninham and V. A. Parsegian, *J. Chem. Phys.* **53**, 3398 (1970).
  - [13] T. Varpula and T. Poutanen, *J. Appl. Phys.* **55**, 4015 (1984).
  - [14] M. S. Tomaš, *Phys. Rev. A* **51**, 2545 (1995).
  - [15] H. Rigneault, S. Robert, C. Begon, B. Jacquier, and P. Moretti, *Phys. Rev. A* **55**, 1497 (1997).
  - [16] P. K. Rekdal, S. Scheel, P. L. Knight, and E. A. Hinds, *Phys. Rev. A* **70**, 013811 (2004).
  - [17] Chen-To Tai, *Dyadic Green's Functions in Electromagnetic Theory* (Intext Educational Publishers, Scranton, 1971).
  - [18] J. A. Stratton, *Electromagnetic Theory* (Wiley-IEEE Press, New York, New Edition 2007).

- [19] K. L. Kliewer and R. Fuchs, *Phys. Rev.* **153**, 498 (1967).
- [20] N. W. Ashcroft and N. D. Mermin, *Solid State Physics* (Harcourt, Fort Worth, 1976).
- [21] P. Grosse, *Freie Elektronen in Festkörpern* (Springer-Verlag, Berlin 1979).
- [22] R. S. Kohlman, J. Joo, Y. Z. Wang, J. P. Pouget, H. Kaneko, T. Ishiguro, and A. J. Epstein, *Phys. Rev. Lett.* **74**, 773 (1995).
- [23] J. D. Jackson, *Classical Electrodynamics*, 3rd ed. (John Wiley, New York, 1998).
- [24] E. M. Lifshitz and L. P. Pitaevskii, *Statistical Physics, Part 2*. Landau and Lifshitz, Course of Theoretical Physics, Vol. 9 (Butterworth-Heinemann, Oxford, 1980).
- [25] M. Janowicz, D. Reddig, and M. Holthaus, *Phys. Rev. A* **68**, 043823 (2003).
- [26] I. Dorofeyev, H. Fuchs, and K. Sobakinskaya, *Central European Journal of Physics* **3**, 351 (2005).
- [27] S.-A. Biehs, D. Reddig, and M. Holthaus, *Thermal near fields of coated dielectrics* (in preparation).
- [28] W. Woltersdorff, *Z. Phys.* **91**, 230 (1934).
- [29] S. Bauer, *Am. J. Phys.* **60**, 257 (1992).
- [30] G. D. Mahan and D. T. F. Marple, *Appl. Phys. Lett.* **42**, 219 (1983).
- [31] C. Henkel and K. Joulain, *Appl. Phys. B* **84**, 61 (2006).
- [32] H. Raether, *Excitation of Plasmons and Interband transitions by Electrons*, Springer Tracts in Modern Physics **88** (Springer, Berlin, 1980).
- [33] P. Fan, K. Yi, J.-D. Shao, and Z.-X. Fan, *J. Appl. Phys.* **95**, 2527 (2004).
- [34] I. A. Dorofeyev, *J. Phys. D: Appl. Phys.* **31**, 600 (1998).
- [35] J.-P. Mulet, K. Joulain, R. Carminati, and J.-J. Greffet, *Appl. Phys. Lett.* **78**, 2931 (2001).
- [36] A. Kittel, W. Müller-Hirsch, J. Parisi, S.-A. Biehs, D. Reddig, and M. Holthaus, *Phys. Rev. Lett.* **95**, 224301 (2005).
- [37] I. Dorofeyev, *The van der Waals interaction of microparticles with a substrate characterized by a nonlocal response* (Preprint, Institute for Physics of Microstructures, Nizhny Novgorod, 2006).

